Title

Chronic hindbrain administration of oxytocin elicits weight loss in male diet-induced obese mice

Journal

AJP Regulatory Integrative and Comparative Physiology, 320(4)

ISSN

0363-6119

Authors

Edwards, Melise M
Nguyen, Ha K
Herbertson, Adam J
et al.

Publication Date

2021-04-01

DOI

10.1152/ajpregu.00294.2020

Peer reviewed

AMERICAN JOURNAL OF PHYSIOLOGY
REGULATORY, INTEGRATIVE AND COMPARATIVE PHYSIOLOGY

Am J Physiol Regul Integr Comp Physiol 320: R471–R487, 2021.
First published January 20, 2021; doi:10.1152/ajpregu.00294.2020

RESEARCH ARTICLE

Obesity, Diabetes and Energy Homeostasis

Chronic hindbrain administration of oxytocin elicits weight loss in male diet-induced obese mice

Melise M. Edwards,[1] Ha K. Nguyen,[1] Adam J. Herbertson,[1] Andrew D. Dodson,[1] Tomasz Wietecha,[2,3] Tami Wolden-Hanson,[1] James L. Graham,[4] Kevin D. O'Brien,[3,5] Peter J. Havel,[4,6] and James E. Blevins[1,2]

[1]*Office of Research and Development Medical Research Service, Department of Veterans Affairs Medical Center, Veteran Affairs Puget Sound Health Care System, Seattle, Washington;* [2]*Division of Metabolism, Endocrinology and Nutrition, Department of Medicine, University of Washington School of Medicine, Seattle, Washington;* [3]*UW Medicine Diabetes Institute, University of Washington School of Medicine, Seattle, Washington;* [4]*Department of Nutrition, University of California, Davis, California;* [5]*Division of Cardiology, Department of Medicine, University of Washington School of Medicine, Seattle, Washington; and* [6]*Department of Molecular Biosciences, School of Veterinary Medicine, University of California, Davis, California*

Abstract

Previous studies indicate that oxytocin (OT) administration reduces body weight in high-fat diet (HFD)-induced obese (DIO) rodents through both reductions in food intake and increases in energy expenditure. We recently demonstrated that chronic hindbrain [fourth ventricular (4V)] infusions of OT evoke weight loss in DIO rats. Based on these findings, we hypothesized that chronic 4V OT would elicit weight loss in DIO mice. We assessed the effects of 4V infusions of OT (16 nmol/day) or vehicle over 28 days on body weight, food intake, and body composition. OT reduced body weight by approximately 4.5% ± 1.4% in DIO mice relative to OT pretreatment body weight ($P < 0.05$). These effects were associated with reduced adiposity and adipocyte size [inguinal white adipose tissue (IWAT)] ($P < 0.05$) and attributed, in part, to reduced energy intake ($P < 0.05$) at a dose that did not increase kaolin intake (P = NS). OT tended to increase uncoupling protein-1 expression in IWAT ($0.05 < P < 0.1$) suggesting that OT stimulates browning of WAT. To assess OT-elicited changes in brown adipose tissue (BAT) thermogenesis, we examined the effects of 4V OT on interscapular BAT temperature (T_{IBAT}). 4V OT (1 μg) elevated T_{IBAT} at 0.75 ($P = 0.08$), 1, and 1.25 h ($P < 0.05$) postinjection; a higher dose (5 μg) elevated T_{IBAT} at 0.75-, 1-, 1.25-, 1.5-, 1.75- ($P < 0.05$), and 2-h ($0.05 < P < 0.1$) postinjection. Together, these findings support the hypothesis that chronic hindbrain OT treatment evokes sustained weight loss in DIO mice by reducing energy intake and increasing BAT thermogenesis at a dose that is not associated with evidence of visceral illness.

brown adipose tissue; obesity; oxytocin; thermogenesis; white adipose tissue

INTRODUCTION

There is growing evidence to suggest that the hypothalamic peptide, oxytocin (OT), is important in the control of overall energy balance (1–4). OT has been shown to reduce food intake, elicit weight loss, and/or reduce body weight gain in male and/or female diet-induced obese (DIO) (5–10) and genetically obese mice and rats (9, 11–16). Of translational importance is the finding that OT can reduce food intake and/or body weight in DIO nonhuman primates (17) and obese and overweight humans (18–21) highlighting that OT's effects on energy balance are well conserved across species.

Although it is understood that OT's ability to elicit weight loss in mice is due, in part, to its ability to reduce food intake, it is becoming clear that other mechanisms can also be a contributing factor. OT-elicited effects on body weight in mice exceed that of pair-fed controls (22) suggesting that reductions in food intake do not fully explain OT-elicited weight loss. In addition, acute third ventricular (3V) or subcutaneous administration of OT increases energy expenditure (EE) in mice (23, 24). Although brown adipose tissue (BAT) thermogenesis is important in the control of EE (for review see Refs. 25, 26), it is unclear whether OT's effects of OT on EE result from activation of BAT thermogenesis. Sutton et al. (27) demonstrated that use of designer drugs (DREADDs) technology to chemogenetically activate paraventricular nucleus (PVN) OT neurons increases both EE and interscapular brown adipose tissue (BAT) temperature (T_{IBAT}) in *Oxytocin-*

Correspondence: J. E. Blevins (jeblevin@u.washington.edu).
Submitted 20 October 2020 / Revised 15 January 2021 / Accepted 16 January 2021

Ires-Cre mice. In addition, Yuan et al. (28) recently reported that peripheral administration of OT promotes BAT differentiation in vitro and the expression of genes involved in thermogenesis in interscapular BAT (IBAT) in high-fat diet (HFD)-fed mice. Furthermore, reduced OT signaling is associated with obesity (24, 29–31), reductions of EE (23, 24, 31, 32), and deficits in BAT thermogenesis (32–35) in mice. Collectively, these findings support a role for increased BAT thermogenesis in OT-elicited weight loss in mice.

The OT receptor (OTR) populations that contribute to the effects of OT on BAT thermogenesis and EE in mice remain uncertain. The majority of studies have examined the effects of acute administration of OT in mice on BAT thermogenesis and EE when administered into the third ventricle (3V) (10, 23, 24). However, this route of administration potentially allows OT access to OTRs in the forebrain, midbrain, and hindbrain. Here, we sought to clarify the role of hindbrain OTRs on energy balance in the mouse model by *1*) determining if hindbrain OTRs contribute to the effects of chronic OT to reduce body weight and adiposity in DIO mice and *2*) measuring the response to acute fourth ventricular (4V) OT on T_{IBAT} (as functional readout of BAT thermogenesis).

Our findings demonstrate that chronic hindbrain (4V) administration of OT reduces HFD consumption at a dose that did not increase kaolin intake (marker of visceral illness) in a mouse model of diet-induced obesity. These effects were associated with reductions of body fat mass, adipocyte size, and plasma leptin concentrations. Furthermore, we determined that hindbrain administration of OT elevates uncoupling protein-1 (UCP-1) expression in inguinal white adipose tissue (IWAT) of both DIO and chow-fed control mice, which suggests that hindbrain OT treatment may be associated with browning of WAT. We also confirm that hindbrain OT administration stimulates BAT thermogenesis in mice. Collectively, these findings support the hypothesis that chronic hindbrain OT treatment produces sustained weight loss in DIO mice by reducing energy intake and increasing BAT thermogenesis at a dose that is not associated with visceral illness.

METHODS

Animals

Adult male C57BL/6J mice (≈5.25–6.5 mo/25.7–51.3 g) were obtained from The Jackson Laboratory (Bar Harbor, ME). All animals were housed individually in Plexiglas cages in a temperature-controlled room (22 ± 2°C) under a 12:12-h light-dark cycle. All mice were maintained on a 6 AM/6 PM light cycle with the exception of *study 2B* where we examined the impact of OT administration during the late-light cycle on IBAT temperature (T_{IBAT}) (1 AM/1 PM). Mice had ad libitum access to water and either a HFD providing 60% kcal from fat (~6.8% kcal from sucrose and 8.9% of the diet from sucrose) (Research Diets, D12492i, New Brunswick, NJ) or a low-fat chow diet containing 16% [5LG4 (Lab Diet); ~0.79% diet from sucrose] kcal from fat, respectively, unless otherwise stated. Kaolin pellets were also purchased from Research Diets, Inc. The research protocols were approved both by the Institutional Animal Care and Use Committee of the Veterans Affairs Puget Sound Health Care System (VAPSHCS) and the University of Washington in accordance with NIH Guidelines for the Care and Use of Animals.

Drug Preparation

Fresh solutions of OT acetate salt (Bachem Americas, Inc., Torrance, CA) were prepared on the day of each experiment. OT was solubilized in sterile water.

4V cannulations for acute injections.

Animals were implanted with a cannula (P1 Technologies, Roanoke, VA) that was directed toward the 4V as previously described (5, 36, 37). Briefly, mice under isoflurane anesthesia were placed in a stereotaxic apparatus with the incisor bar positioned 4.5 mm below the interaural line. A 26-gauge cannula (P1 Technologies) was stereotaxically positioned into the 4V (5.9 mm caudal to bregma; 0.4 mm lateral to the midline, and 2.7 mm ventral to the skull surface) and secured to the surface of the skull with dental cement and stainless steel screws.

4V cannulations for chronic infusions.

Mice were implanted with a cannula within the 4V with a side port that was connected to an osmotic minipump (model 2004, DURECT Corporation) as previously described (10, 38). Mice under isoflurane anesthesia were placed in a stereotaxic apparatus with the incisor bar positioned 4.5 mm below the interaural line. A 30-gauge cannula (P1 Technologies) was stereotaxically positioned into the 4V (5.9 mm caudal to bregma; 0.4 mm lateral to the midline, and 3.7 mm ventral to the skull surface) and secured to the surface of the skull with dental cement and stainless steel screws. A 1.2 in. piece of plastic Tygon Microbore Tubing (0.020 in. × 0.060 in. OD; Cole-Parmer) was tunneled subcutaneously along the midline of the back and connected to the 21-gauge sidearm osmotic minipump-cannula assembly. A stainless steel 22-gauge pin plug (Instech Laboratories, Inc.) was temporarily inserted at the end of the tubing during a 2-wk postoperative recovery period, after which it was replaced by an osmotic minipump (DURECT Corporation) containing saline or OT. Mice were treated with the analgesic ketoprofen (5 mg/kg; Fort Dodge Animal Health) and the antibiotic enrofloxacin (5 mg/kg; Bayer Healthcare LLC., Animal Health Division Shawnee Mission, KS) at the completion of the 4V cannulations and were allowed to recover at least 10 days before implantation of osmotic minipumps.

Implantation of temperature transponders underneath IBAT.

Animals were anesthetized with isoflurane and had the dorsal surface along the upper midline of the back shaved. The area was subsequently scrubbed with 70% ethanol followed by betadine swabs to sterilize/clean the area before a 1 in. incision was made at the midline of the interscapular area. The temperature transponder (14 mm long/2 mm wide) (HTEC IPTT-300; Bio Medic Data Systems, Inc., Seaford, DE) was implanted underneath both IBAT pads as previously described (10, 39, 40) and secured in place by suturing it to the brown fat pad with sterile silk suture. HTEC IPTT-300 transponders were used in place of IPTT-300 transponders to enhance accuracy in our measurements. The IPTT-300 transponders are specified to be accurate to ±0.4°C between

35°C and 39°C (±1.0°C between 32°C and 42°C), whereas the HTEC IPTT-300 transponders are accurate to ±0.2°C between 32°C and 42°C (personal communication with Geoff Hunt from Bio Medic Data Systems). The interscapular incision was closed with Nylon sutures (5-0), which were removed in awake animals 10–14 days after surgery.

Acute 4V injections and measurements of T_{IBAT}.

OT (or saline vehicle; 1 μL injection volume) was administered immediately before the start of the dark cycle following 4 h of food deprivation. Animals remained without access to food for an additional 4 h during the course of the T_{IBAT} measurements to prevent the confounding effects of diet-induced thermogenesis on T_{IBAT}. A handheld reader (DAS-8007-IUS Reader System; Bio Medic Data Systems, Inc.) was used to collect measurements of T_{IBAT}. The 4V injections were administered at 1 μL/min using an injection pump (Harvard Apparatus Pump II Elite; Harvard Apparatus, Holliston, MA) via a 33-gauge injector (P1 Technologies) connected by polyethylene 20 tubing to a 10-μL Hamilton syringe. Animals underwent all treatments (unless otherwise noted) in a randomized order separated by at least 48 h between treatments.

Body composition.

Determinations of lean body mass and fat mass were made on un-anesthetized mice by quantitative magnetic resonance using an EchoMRI 4-in-1-700 instrument (Echo Medical Systems, Houston, TX) at the VAPSHCS Rodent Metabolic Phenotyping Core. Measurements were taken before 4V cannulations and minipump implantations as well as at the end of the infusion period.

Study Protocols

Study 1A: Effects of chronic 4V OT infusions on energy intake, body weight, and body composition in male chow-fed and DIO mice.

Mice were fed ad libitum and maintained on chow or HFD for ~5 mo before receiving implantations of 4V cannulas and 28-day minipumps to infuse vehicle or OT (16 nmol/day) over 28 days, respectively. This dose was selected because it was found to be effective at reducing body weight when given into the 3V in DIO mice (10). Daily energy intake and body weight were recorded manually on *days 1–28*.

Study 1B: Effect of chronic 4V OT infusions on kaolin consumption in male DIO mice.

The amount of kaolin intake (g) was assessed across 28 days following implantation of minipumps containing vehicle (saline) or OT (16 nmol/day) in a subset of animals from *Study 1A*.

Study 2A: Effects of acute 4V OT administration during early-light cycle on T_{IBAT} in male chow-fed mice.

A separate group of mice was implanted with 4V cannulas and temperature transponders. Following adaptation to a 4-h fast (fast started at 6 AM) and handling, 4-h fasted mice received 4V injections of either vehicle or OT (1, 5 μg/μL) during the early-light cycle [injections between 9:45 and 10 AM (lights off at 6 PM)] in a crossover design at 48-h intervals such that each animal served as its own control. T_{IBAT} was measured at baseline (−2 h; 8:00 AM), immediately before 4V injections (0 h), and at 0.25-, 0.5-, 0.75-, 1-, 1.25-, 1.5-, 2-, 3-, 4-, and 24-h postinjection (10:00 AM). These doses were selected because they were found to be effective at elevating T_{IBAT} when given into the 3V in chow-fed mice (10).

Study 2B: Effects of acute 4V OT administration during late-light cycle on T_{IBAT} in male chow-fed mice.

The same mice from *study 2A* were also used in *study 2B*. Study parameters were identical to *study 2A* with the exception that the fast started at 9:00 AM and 4-h fasted mice received 4V injections of either vehicle or OT (1, 5 μg/μL) during the late-light cycle [injections between 12:45 and 1 PM (lights off at 1 PM)] in a crossover design at 48-h intervals such that each animal served as its own control. T_{IBAT} was again measured at baseline (−2 h; 11:00 AM), immediately before 4V injections (0 h), and at 0.25-, 0.5-, 0.75-, 1-, 1.25-, 1.5-, 2-, 3-, 4-, and 20-h postinjection (9:00 AM).

Study 2C: Effects of acute 4V OT administration during early-light cycle on T_{IBAT} in male DIO mice.

Study parameters were identical to *study 2A* with the exception that DIO mice were used in place of lean mice. T_{IBAT} was again measured at baseline (−2 h; 8:00 AM), immediately before 4V injections (0 h), and at 0.25-, 0.5-, 0.75-, 1-, 1.25-, 1.5-, 2-, 3-, 4-, and 20-h postinjection (10:00 AM).

Blood collection.

Blood was collected from 3-h fasted mice toward the early-light cycle within a 2-h window (10:00 AM–12:00 pm/6 AM/6 PM light cycle) as previously described in DIO CD IGS rats and mice (5, 10). Treatment groups were counterbalanced at the time of euthanasia to avoid time of day bias. Blood samples [up to 0.5 mL (mice)] were collected immediately before transcardial perfusion by cardiac puncture in chilled K2 EDTA Microtainer Tubes (Becton Dickinson, Franklin Lakes, NJ). Whole blood was centrifuged at 6,000 rpm for 1.5 min at 4°C; plasma was removed, aliquoted, and stored at −80°C for subsequent analysis.

Adipose tissue processing for adipocyte size and UCP-1 analysis.

Mice from *Study 1A* were euthanized at the end of the infusion period following a 3-h fast. Mice were euthanized with intraperitoneal injections of ketamine cocktail [ketamine hydrochloride (390 mg/kg), xylazine (26.4 mg/kg) in an injection volume up to 1 mL/mouse] and transcardially exsanguinated with PBS followed by perfusion with 4% paraformaldehyde in 0.1 M PBS. Inguinal white adipose tissue (IWAT) and epididiymal white adipose tissue (EWAT) was dissected and placed in 4% paraformaldehyde-PBS for 24 h and then placed in 70% ethanol (EtOH) before paraffin embedding. Sections (5 μm) sampled were obtained using a rotary microtome, slide-mounted using a floatation water bath (37°C), and baked for 30 min at 60°C to give ~15–16 slides/fat depot with 2 sections/slide.

Adipocyte size analysis and UCP-1 staining.

Adipocyte size analysis was performed on deparaffinized and digitized IWAT and EWAT sections collected from mice

used in *Study 1A*. The average cell area from two randomized photomicrographs was determined using the built-in particle counting method of ImageJ software (National Institutes of Health, Bethesda, MD). Fixed [4% paraformaldehyde (PFA)], paraffin-embedded adipose tissue was sectioned and stained with a primary rabbit anti-UCP-1 antibody [1:100; Abcam, Cambridge, MA (No. ab155117/RRID: AB_2783809)] as has been previously described in HFD-fed *Ldlr*$^{-/-}$ mice (41) and in HFD-fed C57BL/6 (42) and C57BL/6J mice (43). Immunostaining specificity controls included omission of the primary antibody and replacement of the primary antibody with normal rabbit serum at the same dilution as the respective primary antibody. Area quantification for UCP1 staining was performed on digital images of immunostained tissue sections using image analysis software (Image Pro Plus software, Media Cybernetics, Rockville, MD). Slides were visualized using brightfield on an Olympus BX51 microscope (Olympus Corporation of the Americas; Center Valley, PA) and photographed using a Canon EOS 5D SR DSLR (Canon U.S.A., Inc., Melville, NY) camera at ×100 magnification. Values for each tissue within a treatment were averaged to obtain the mean of the treatment group.

Plasma hormone measurements.

Plasma leptin and insulin were measured using electrochemiluminescence detection [Meso Scale Discovery (MSD), Rockville, MD] using established procedures (10, 44). Intra-assay coefficient of variation (CV) for leptin was 5.9% and 1.6% for insulin. The range of detectability for the leptin assay is 0.137–100 ng/mL and 0.069–50 ng/mL for insulin. Plasma fibroblast growth factor-21 (FGF-21) (R&D Systems, Minneapolis, MN) and irisin (AdipoGen, San Diego, CA) levels were determined by enzyme-linked immunosorbent assay (ELISA). The intra-assay CV for FGF-21 and irisin were 2.2% and 9.1%, respectively; the ranges of detectability were 31.3–2,000 pg/mL (FGF-21) and 0.078–5 μg/mL (irisin). Plasma adiponectin was also measured using ELISA [Millipore Sigma (Burlington, MA)] using established procedures (10, 44). Intra-assay CV for adiponectin was 3.7%. The range of detectability for the adiponectin assay is 2.8–178 ng/mL. The data were normalized to historical values using a pooled plasma quality control sample that was assayed in each plate.

Blood glucose and lipid measurements.

Blood was collected for glucose measurements by tail vein nick and measured with a glucometer using the AlphaTRAK 2 blood glucose monitoring system (Abbott Laboratories, Abbott Park, IL) (45). Total cholesterol (TC) [Fisher Diagnostics (Middletown, VA)] and free fatty acids (FFAs) [Wako Chemicals USA, Inc., Richmond, VA)] were measured using enzymatic-based kits. Intra-assay CVs for TC and FFAs were 1.4% and 2.3%, respectively. These assay procedures have been validated for rodents (46).

Transponder placement.

All temperature transponders were confirmed to have remained underneath the IBAT depot at the conclusion of the study.

Histological verification of coordinate to target 4V in C57BL/6J mice.

We initially verified the coordinate to target the 4V in a subset of C57BL/6J mice following postmortem ink administration.

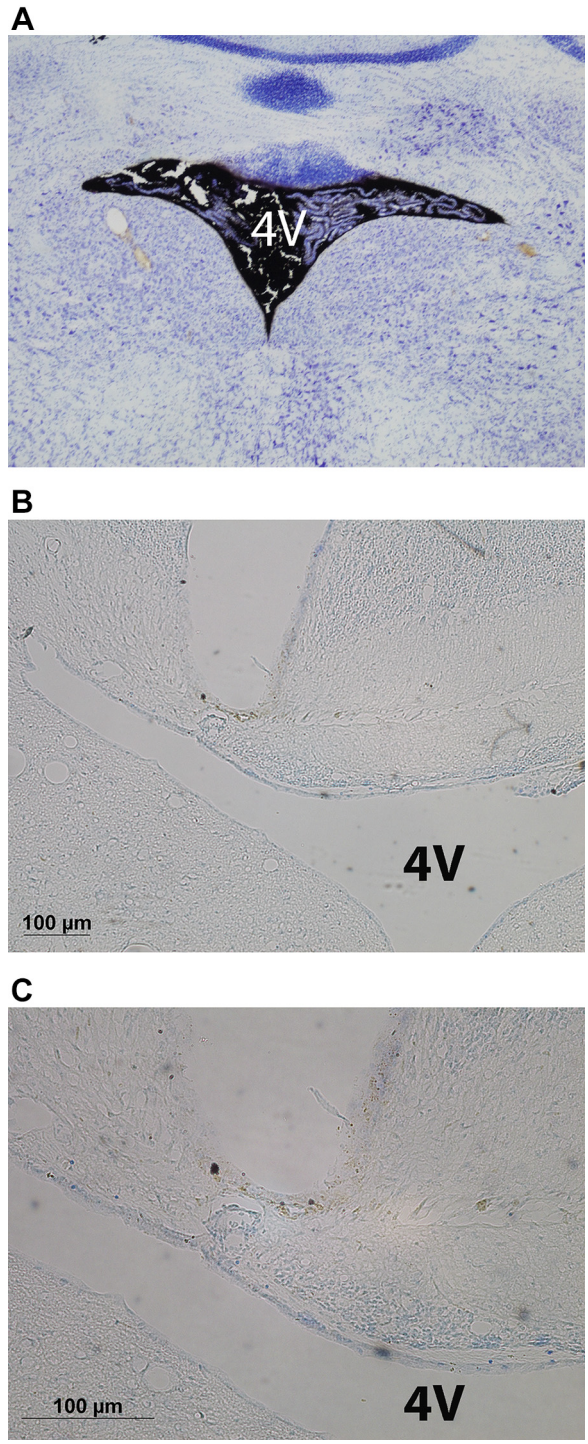

Figure 1. Photomicrograph of coronal section of the mouse brain showing ink distribution in the fourth ventricular (4V) (*A*) following postmortem 4V ink injections into a C57BL/6J mouse (×10 magnification) and cannula tract immediately dorsal to the 4V from an oxytocin (OT)-treated diet-induced obese (DIO) C57BL/6J mouse at ×10 (*B*) and ×20 (*C*) magnification.

Brains from a subset of animals from *study 1A* were examined to verify accurate placements surrounding the 4V. The procedure for histological verification of injection sites has been described previously (47–50). Briefly, brains were frozen by submerging for 10–15 s in isopentane. Coronal cryostat sections (14 or 24 μm) were mounted on microscope slides and stored frozen until staining with Cresyl violet (Fig. 1). Slides were analyzed using brightfield on a Nikon 80i microscope (Nikon Instruments, Melville, NY) and images obtained using NIS Elements and Nikon Digital Sight Series color camera (DS-Fi1; Nikon Instruments). All measurements were made using a ×20 objective lens. Digital RGB images were exported to Photoshop (Adobe, Tucson, AZ). Injection sites examined were found to be located within a 0.2 mm beyond boundary of the 4V. Although, we did not measure the area of the necrotic tissue based on the observations that at higher magnification revealed no obvious visual differences between groups with respect to histological and morphological appearances.

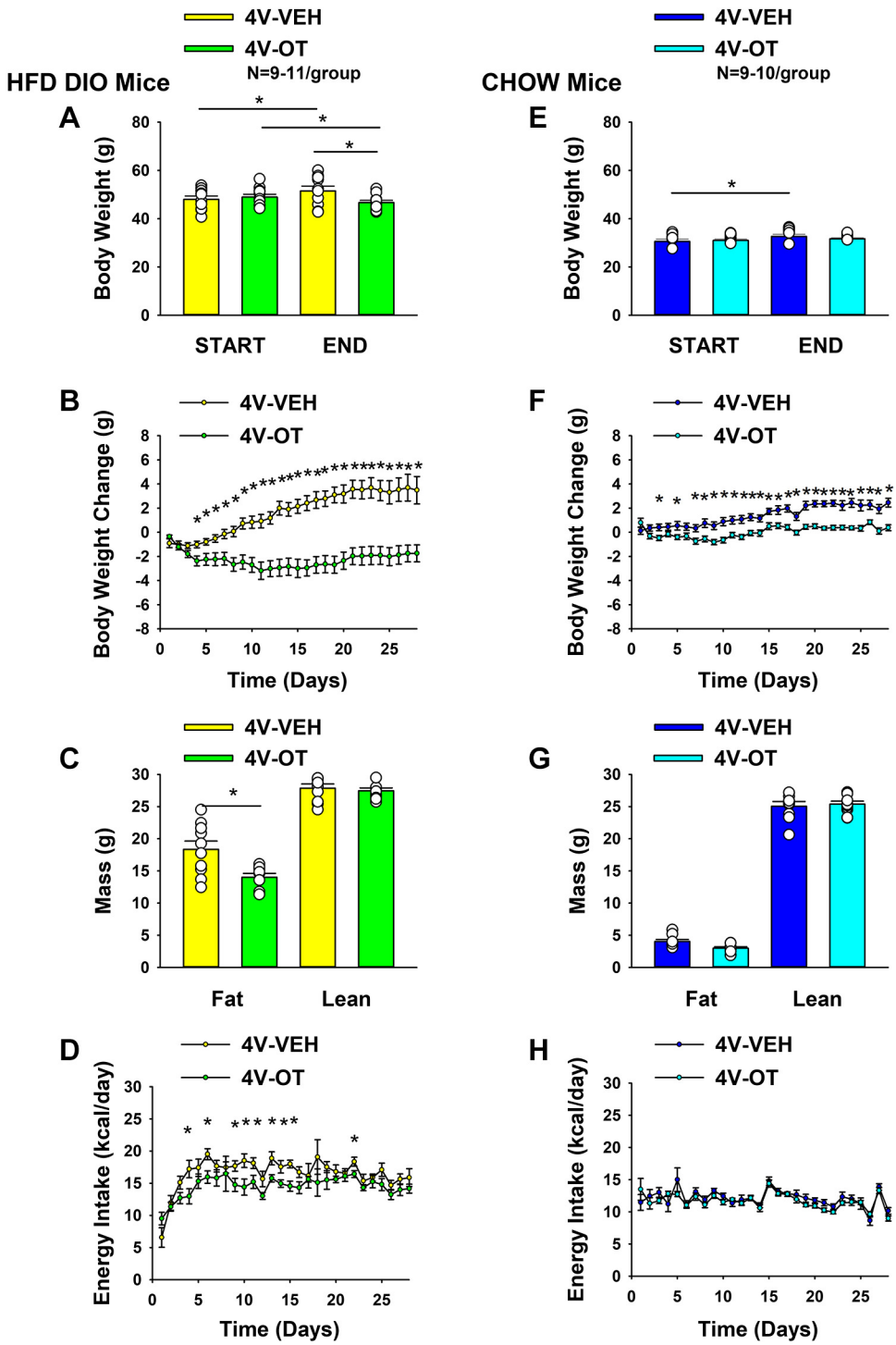

Figure 2. Effects of chronic fourth ventricular (4V) oxytocin (OT) infusions on body weight, body weight gain, body composition, and energy intake in male chow-fed and diet-induced obese (DIO) mice. Ad libitum-fed mice were either maintained on high-fat diet (HFD) (60% kcal from fat; n = 9–11/group) or chow (n = 9–10/group) for approximately 5 mo before receiving continuous infusions of vehicle or OT (16 nmol/day). *A* and *E*: change in body weight in HFD-fed DIO or chow-fed control animals; *B* and *F*: change in body weight gain in HFD-fed DIO or chow-fed control animals; *C* and *G*: fat mass and lean mass in HFD-fed DIO or chow-fed control animals; *D* and *H*: daily energy intake (kcal/day) in HFD-fed DIO or chow-fed control animals. One-way ANOVA; data are expressed as means ± SE. *P < 0.05 OT vs. vehicle or baseline (pretreatment; A and *E*).

The brain tissue appeared normal in all cases, as compared with brain tissue from reference material from mice and rats that had received acute injections or continuous infusions of vehicle or OT prepared in a similar way. Nothing was noted visually in either group that suggested damage.

Statistical Analyses

All results are expressed as means ± SE. Comparisons between multiple groups involving between-subjects designs were made using one- or two-way ANOVA as appropriate, followed by a post hoc Fisher's least significant difference test. Comparisons involving within-subjects designs were made using a one-way repeated-measures ANOVA followed by a post hoc Fisher's least significant difference test. Analyses were performed using the statistical program SYSTAT (Systat Software, Point Richmond, CA). Differences were considered significant at $P < 0.05$, two-tailed.

RESULTS

Study 1A: Effects of Chronic 4V OT Infusions on Energy Intake, Body Weight, and Body Composition in Male Chow-Fed and DIO Mice

To determine whether the weight-reducing effect of chronic 4V OT infusion is observed in DIO mice, we examined the effects of 4V OT on energy intake, body weight, and body composition in age-matched DIO and chow-fed C57BL/6J mice. By design, DIO mice weighed more (48.5 ± 0.9 g) and had increased adiposity (18.6 ± 0.7 g) relative to chow-fed mice (body weight 32.4 ± 0.4 g; fat mass 4.0 ± 0.4 g) ($P < 0.05$) at baseline (after maintenance on either chow or HFD for ~5 mo). Mice were also matched for body weight, fat mass, and weight change post-4V cannulations before minipump implantations within each dietary group.

HFD.

4V OT treatment induced reductions of body weight (≈4.7% relative to pretreatment in OT-treated mice or ≈9.3% relative to vehicle-treated mice; $P < 0.05$) (Fig. 2*A*) and weight gain (Fig. 2*B*) throughout the 28-day infusion period [$F(1,17) = 20.190$; $P < 0.001$)] with significant reductions in daily weight gain evident on *days 4–28* ($P < 0.05$; Fig. 2*B*). There was a significant main effect of OT to reduce fat mass (Fig. 2*C*; $P < 0.05$) with no effect on lean body mass (P = NS), as was observed in DIO rats, effects that were mediated, at least in part, by a modest reduction of energy intake (Fig. 2*D*; $P < 0.05$).

Chow.

Similar to our previously reported observations in rats (10), the weight-reducing effect of 4V OT in HFD-fed DIO mice was not observed in mice fed standard chow (Fig. 2*E*; P = NS), although a slight attenuation of weight gain relative to 4V vehicle-treated controls was observed over the 28-day period (Fig. 2*F*; $P < 0.05$). This modest effect was not associated with significant effects on fat mass or lean mass (Fig. 2*G*; P = NS) or energy intake relative to vehicle-treated controls (Fig. 2*H*).

Two-way ANOVA revealed a significant diet and drug interactive effect indicating that 4V OT produced a more preferential reduction of body weight gain in HFD-fed mice compared with chow-fed mice across *days 9–28* ($P < 0.05$). In addition, OT produced a preferential reduction of energy intake in HFD-fed rats relative to chow-fed rats across *days 4*, *6*, *11*, *13*, and *15* ($P < 0.05$).

Two-way ANOVA revealed a significant main effect of 4V OT (drug) [$F(1,35) = 13.007$, $P = 0.001$] and diet [$F(1,35) = 89.433$, $P < 0.001$] to impact fat mass as well as significant interactive effect of the 4V OT to preferentially reduce fat mass in HFD-fed mice [$F(1,35) = 4.905$, $P = 0.033$]. These findings extend our previous findings in the DIO rat model and indicate that hindbrain (4V) administration of OT preferentially reduces fat mass in DIO mice relative to chow-fed mice.

Overall, these findings demonstrate a preferential effect of OT to reduce energy intake and produce sustained weight

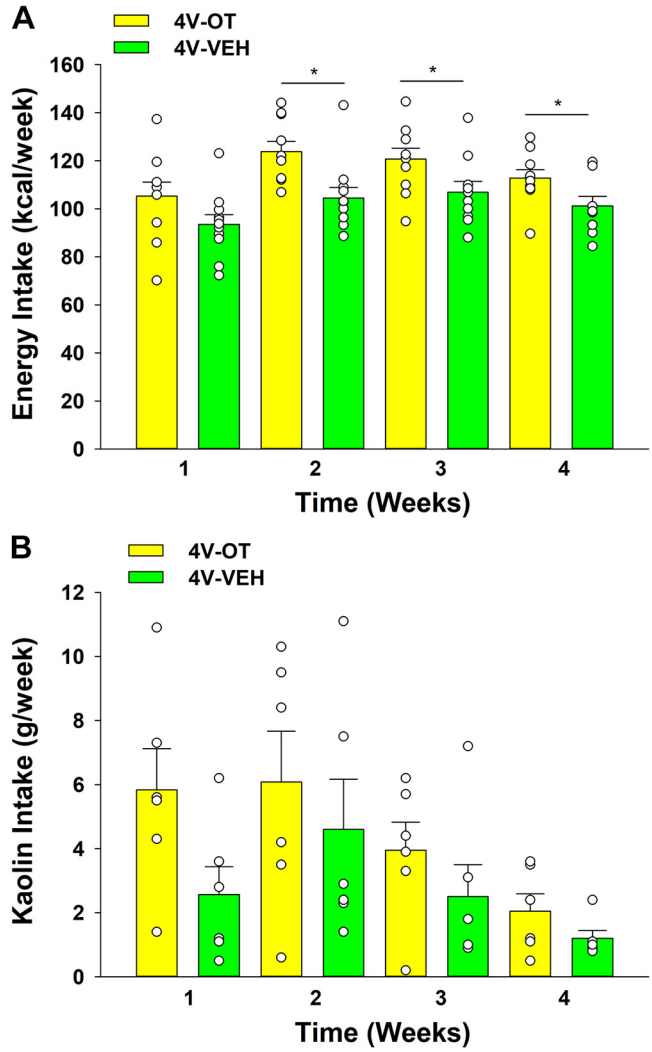

Figure 3. Effects of chronic fourth ventricular (4V) oxytocin (OT) infusions on weekly energy intake and kaolin intake in male diet-induced obese (DIO) mice. Ad libitum-fed mice were maintained on high-fat diet (HFD) and infused with 4V vehicle or OT (16 nmol/day). Weekly energy intake (*A*) and kaolin consumption (*B*) are presented (n = 6/group). One-way ANOVA; data are expressed as means ± SE. *$P < 0.05$ OT vs. vehicle treatment.

loss by decreasing fat mass while sparing lean mass in DIO mice at a dose that was largely ineffective in chow-fed mice.

Study 1B: Effect of Chronic 4V OT Infusions on Kaolin Consumption in Male DIO Mice

To determine whether the weight-reducing effect of chronic 4V OT infusion observed in DIO mice was associated with visceral illness, we examined the intake of kaolin diet, which is commonly used to assess malaise or aversion in rodent populations (51–54) including mice (55). These effects do not appear to result from an aversive effect of 4V OT, since there was no effect on kaolin consumption (relative to vehicle-treated DIO control mice; n = 6/group) over the 28-day measurement period (P = NS; Fig. 3). Overall, these findings demonstrate that the response of DIO mice to 4V OT is similar to our previous findings in DIO rats (10) and they extend previous evidence that neither acute nor chronic 3V administration of OT affects kaolin consumption (5, 10, 23).

Adipocyte size.

OT significantly reduced adipocyte size from IWAT in DIO mice [$F(1,18) = 9.582$, $P = 0.006$], but it did not significantly reduce adipocyte size from IWAT in chow-fed mice [$F(1,17) = 0.822$, $P = 0.377$] (Fig. 4, *A–D* and Fig. 5*A*). OT did not significantly reduce adipocyte size from EWAT in either DIO mice [$F(1,18) = 0.004$, $P = 0.951$] or chow-fed mice [$F(1,17) = 0.233$, $P = 0.636$] (Fig. 4, *E–H* and Fig. 5*B*).

Two-way ANOVA revealed a significant main effect of 4V OT (drug) [($F(1,35) = 9.060$, $P = 0.005$] and diet [F

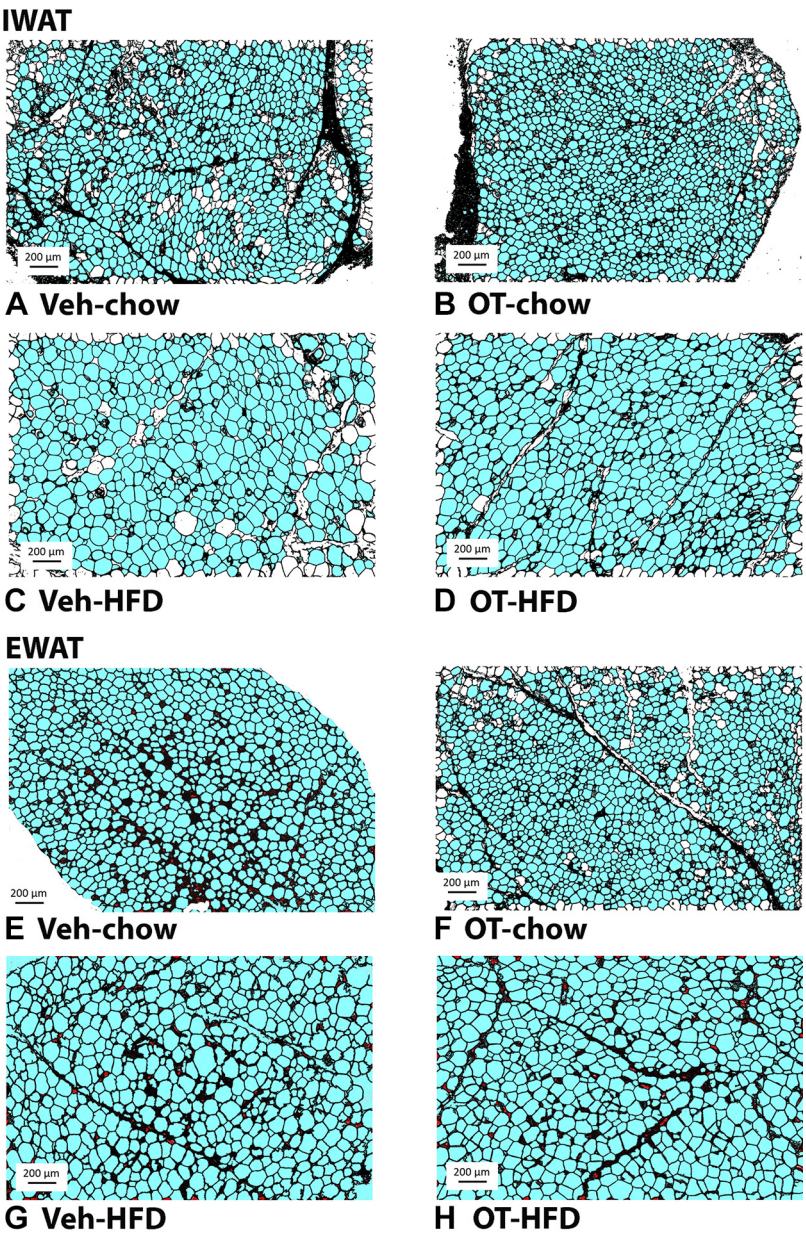

Figure 4. *A–H*: effects of chronic fourth ventricular (4V) oxytocin (OT) infusions on adipocyte size in inguinal white adipose tissue (IWAT) and epididiymal white adipose tissue (EWAT) in male chow-fed and diet-induced obese (DIO) mice. Adipocyte size was analyzed using ImageJ. Images were taken from fixed (4% paraformaldehyde) paraffin-embedded sections (5 μm) containing IWAT (*A–D*) or EWAT (*E–H*) in chow-fed or high-fat diet (HFD)-fed mice treated with OT or vehicle. *A* and *E*: Veh-chow. *B* and *F*: OT-chow. *C* and *G*: Veh-HFD. *D* and *H*: OT-HFD; (*A–H*) all visualized at ×100 magnification.

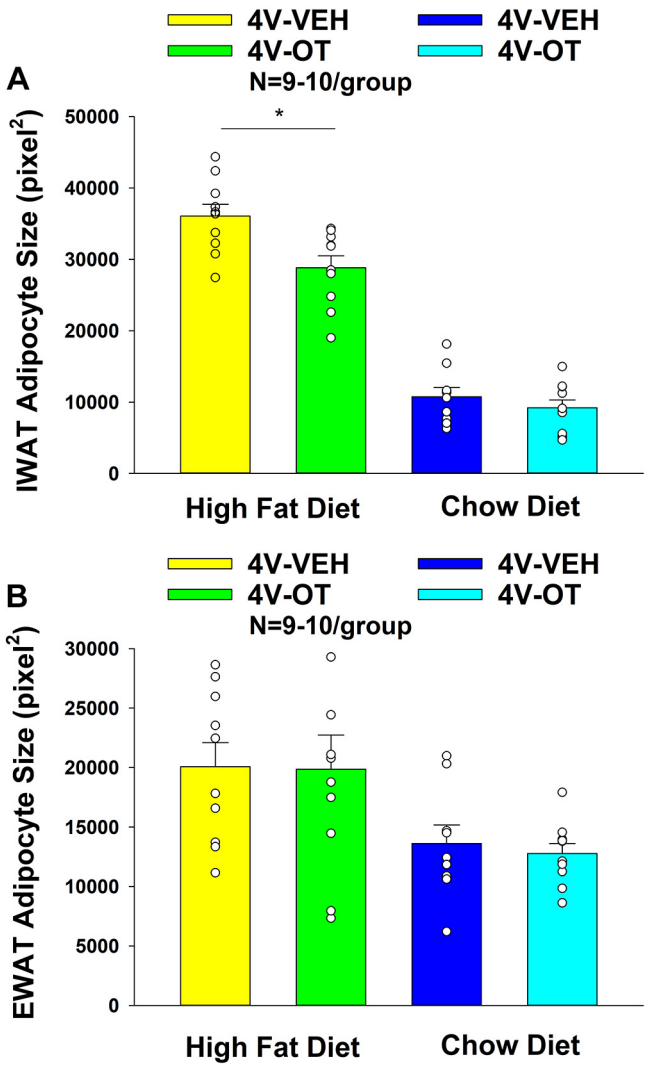

Figure 5. *A* and *B*: effects of chronic fourth ventricular (4V) oxytocin (OT) infusions on adipocyte size in inguinal white adipose tissue (IWAT) and epididiymal white adipose tissue (EWAT) in male chow-fed and diet-induced obese (DIO) mice. *A*: adipocyte size (pixel^2) was measured in IWAT from mice that received chronic 4V infusion of OT (16 nmol/day) or vehicle (n = 9–10/group). *B*: adipocyte size was measured in EWAT from mice that received chronic 4V infusion of OT (16 nmol/day) or vehicle (n = 9–10/group). One-way ANOVA; data are expressed as means ± SE. *P < 0.05 OT vs. vehicle.

(1,35) = 237.714, $P < 0.001$] and a near significant interactive effect of the 4V OT and diet to reduce adipocyte size of IWAT [F(1,35) = 3.824, P = 0.059]. These findings extend our previous findings and indicate that hindbrain (4V) administration of OT preferentially reduces IWAT adipocyte size in DIO mice relative to chow-fed mice.

UCP-1 expression.

OT tended to increase UCP-1 from IWAT in DIO mice [F(1,17) = 3.867, P = 0.066] and produced a significant elevation in UCP-1 from IWAT in chow-fed mice [F(1,16) = 6.692, P = 0.02] (Fig. 6, *A–D* and Fig. 7*A*). OT tended to elevate UCP-1 from EWAT in DIO [F(1,16) = 2.051, P = 0.171] and chow-fed mice [F(1,16) = 1.940, P = 0.183] although this did not reach statistical significance (Fig. 6, *E–H* and Fig. 7*B*).

Two-way ANOVA revealed a significant main effect of 4V OT (drug) [(F(1,33) = 9.837, P = 0.004] and diet [F(1,33) = 51.542, $P < 0.001$] and a near significant interactive effect of the 4V OT and diet to increase UCP-1 in IWAT [F(1,33) = 3.602, P = 0.066].

Although OT was effective in stimulating UCP-1 from IWAT in both HFD and chow-fed mice, these findings indicate that hindbrain (4V) administration of OT appears to preferentially increase UCP-1 in IWAT of chow-fed mice relative to DIO mice.

Plasma hormone concentrations.

To characterize the endocrine and metabolic effects of 4V OT in both DIO and chow-fed mice, we measured blood glucose levels and plasma concentrations of leptin, insulin, FGF-21, irisin, adiponectin, TC, and FFAs. At baseline, vehicle-treated DIO animals exhibited increased levels of leptin, insulin, FGF-21, and TC relative to chow-fed vehicle-treated animals ($P < 0.05$; Table 1). As expected, OT treatment was associated with a reduction of plasma leptin in DIO animals (5, 6, 10) (in which fat mass was also reduced), but not in chow-fed control animals. In contrast, OT administration did not significantly alter blood glucose or plasma concentrations of insulin, irisin, TC, or adiponectin in either DIO or chow-fed mice.

Two-way ANOVA revealed a significant main effect of 4V OT (drug) [(F(1,36) = 6.485, P = 0.015] and diet [F(1,36) = 86.598, $P < 0.001$] and a significant interactive effect of the 4V OT and diet to reduce plasma leptin [F(1,36) = 5.374, P = 0.026]. As expected, based on our findings on fat mass, these findings indicate that hindbrain (4V) administration of OT preferentially reduces plasma leptin in DIO mice relative to chow-fed mice.

Study 2A–B: Effects of Acute 4V OT Administration on T_{IBAT} in Male Chow-Fed Mice

Given that reduced energy intake cannot fully explain the ability of either acute (9) or chronic OT (6, 22) to reduce body weight in rodents and the finding that acute administration of OT increases EE in both rodents (23, 24, 56) and nonhuman primates (17), we hypothesized that the anti-obesity effect of OT action in the central nervous system (CNS) involves increased EE. Numerous data suggest that increased activation of BAT is one mechanism that can contribute to increased EE (for review see Refs. 25, 26). Being that changes in both EE and IBAT have been more easily measured in response to acute OT administration (17, 23, 24, 56), we initially sought to determine the extent to which acute administration of OT stimulates BAT thermogenesis (as a surrogate for EE) and whether hindbrain OTRs may be involved in contributing to these effects. Therefore, we measured the effect of acute hindbrain (4V) administration of OT on T_{IBAT} in chow-fed mice.

Study 2A: Early-light cycle treatment.

Consistent with this hypothesis, we found that, similar to our previous findings in the rat model (10), there was a significant main effect of 4V OT to elevate T_{IBAT} at 1- [(F(2,16) = 7.919, $P <$ 0.01], 1.25- [(F(2,16) = 9.074, $P < 0.01$], 1.5- [(F(2,16) = 6.577, $P <$

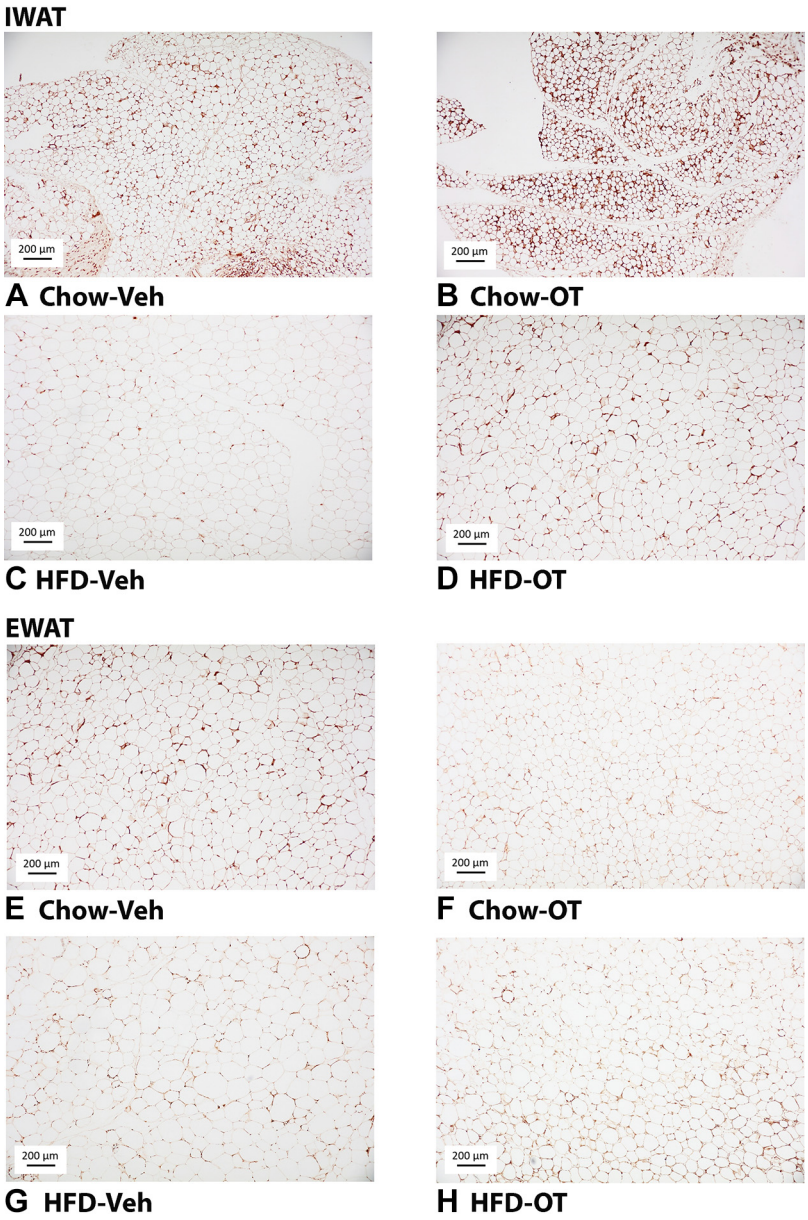

Figure 6. *A–H*: effects of chronic fourth ventricular (4V) oxytocin (OT) infusions on uncoupling protein-1 (UCP-1) in inguinal white adipose tissue (IWAT) and epididiymal white adipose tissue (EWAT) in male chow-fed and diet-induced obese (DIO) mice. UCP-1 was analyzed using ImageJ. Images were taken from fixed (4% paraformaldehyde) paraffin embedded sections (5 μm) containing IWAT (*A–D*) or EWAT (*E–H*) in chow-fed or high-fat diet (HFD)-fed mice treated with OT or vehicle. *A* and *E*: veh-chow. *B* and *F*: OT-chow. *C* and *G*: veh-HFD. *D* and *H*: OT-HFD; *A–H:* all visualized at ×100 magnification.

0.01], and 1.75-h postinjection [($F(2,16) = 5.115$, $P < 0.05$] and there was also a tendency (NS) for 4V OT to elevate T_{IBAT} at 0.75- [($F(2,16) = 3.246$, $P = 0.066$]. We also found a significant effect of time [($F(8,192) = 22.262$, $P < 0.01$] and a significant interactive effect between time and dose [($F(16,192) = 2.530$, $P < 0.01$] across nine time points over the 2-h measurement period.

Specifically, 4V OT also increased T_{IBAT} at both 1 and 5 μg doses throughout the 2-h measurement period in chow-fed mice ($N = 9$/group). Specifically, OT (1 μg) tended to increase T_{IBAT} at 0.75 ($0.05 < P < 0.1$), and significantly elevated T_{IBAT} at both 1- and 1.25-h postinjection ($P < 0.05$). The higher dose (5 μg) of 4V OT increased T_{IBAT} at 0.75-, 1-, 1.25-, 1.5-, and 1.75-h postinjection ($P < 0.05$), whereas it tended to elevate T_{IBAT} at 2-h postinjection relative to vehicle treatment (Fig. 8*A*; $0.05 < P < 0.1$). OT also produced corresponding changes in the change in T_{IBAT} relative to baseline T_{IBAT} at 1-, 1.25-, 1.5-, and 1.75-h postinjection relative to vehicle treatment (Fig. 8*B*).

There was also a significant main effect of 4V OT to elevate T_{IBAT} when the data were averaged over the 2-h posttreatment period [($F(2,16) = 6.231$, $P < 0.05$]. Specifically, 4V OT (5 μg; $P < 0.05$) produced a significant elevation of T_{IBAT} when data were averaged over the 2-h posttreatment period (Fig. 8*C*) whereas the low dose (1 μg) tended to elevate T_{IBAT} (NS; $0.05 < P < 0.01$). Similar to what we observed following 4V administration in the rat model (10), acute 4V OT administration did not produce a significant elevation in T_{IBAT} at 24-h postinjection (P = NS; data not shown).

Study 2B: Late-light cycle treatment.

To assess the extent to which OT elicits changes in BAT thermogenesis when administered at the end of the light cycle,

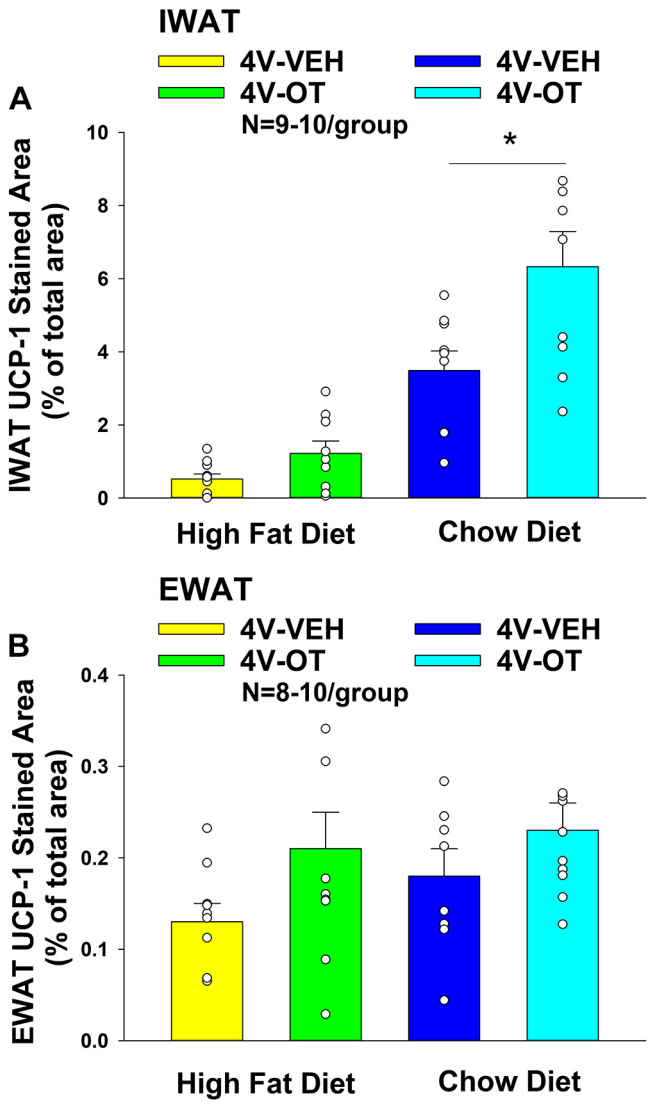

Figure 7. *A* and *B*: effects of chronic fourth ventricular (4V) oxytocin (OT) infusions on uncoupling protein-1 (UCP-1) in inguinal white adipose tissue (IWAT) and epididiymal white adipose tissue (EWAT) in male chow-fed and diet-induced obese (DIO) mice. *A*: UCP-1 staining was quantified in IWAT from mice that received chronic 4V infusion of OT (16 nmol/day) or vehicle (n = 9–10/group). *B*: UCP-1 staining was quantified in EWAT from mice that received chronic 4V infusion of OT (16 nmol/day) or vehicle (n = 8–10/group). One-way ANOVA; data are expressed as means ± SE. *$P < 0.05$ OT vs. vehicle.

we initially examined the effects of acute 4V injections of OT (1, 5 μg/μL) or vehicle on T_{IBAT} in a small cohort of 4-h fasted mice (n = 4/group). Preliminary data indicate that acute 4V injections of OT (5 μg) elevated T_{IBAT} at 1.5- ($P < 0.05$) and 4-h ($0.05 < P < 0.1$) postinjection in mice.

We subsequently confirmed these effects in a larger group of chow-fed mice (N = 10/group). There was a significant main effect of 4V OT (drug) to elevate T_{IBAT} at 0.75- [($F(2,18) = 9.547$, $P < 0.01$], 1- [($F(2,18) = 5.025$, $P < 0.05$], 1.25- [($F(2,18) = 5.701$, $P < 0.05$], and 1.75-h postinjection [($F(2,18) = 4.586$, $P < 0.05$] and there was also a tendency (NS) of 4V OT to elevate T_{IBAT} at 1.5-h postinjection [($F(2,18) = 2.672$, $P = 0.096$]. We also found a significant effect of time [($F(8,216) = 45.790$, $P < 0.01$] but we did not find a significant interactive effect between time and dose [($F(16,216) = 0.944$, P = NS] across nine time points over the 120-min measurement period.

OT (1 μg) increased T_{IBAT} at 0.75-h postinjection, whereas it tended to elevate T_{IBAT} at 1-, 1.25-, and 1.75-h postinjection ($0.05 < P < 0.1$). The higher dose (5 μg) of 4V OT increased T_{IBAT} at 0.75-, 1-, 1.25-, and 1.75-h postinjection ($P < 0.05$), whereas it tended (NS) to elevate T_{IBAT} at both 1.5- ($0.05 < P < 0.1$) and 4-h ($P = 0.05$) postinjection relative to vehicle treatment (Fig. 9*A*). OT also produced a corresponding change in T_{IBAT} relative to baseline T_{IBAT} at 0.75-h postinjection relative to vehicle treatment (Fig. 9*B*). There was also a significant main effect of 4V OT to elevate T_{IBAT} when the data were averaged over the 2-h posttreatment period [($F(2,18) = 7.499$, $P < 0.01$]. Specifically, 4V OT (5 μg; $P < 0.05$) produced a significant elevation of T_{IBAT} when data were averaged over the 2-h posttreatment period (Fig. 9*C*).

When comparing the T_{IBAT} following either vehicle or OT treatment, there were clear differences in the T_{IBAT} response to both, depending on timing of administration. Consistent with our unpublished observations in untreated mice and rats, T_{IBAT} was higher in mice treated with vehicle at the end of the light cycle (1.25-, 1.5-, 1.75-, 2-, 3-, and 4-h postinjection; $P < 0.05$). Similarly, T_{IBAT} was also higher in response to 4V OT when given during the end of the light cycle (2-, 3-, and 4-h postinjection) but this did not reach significance relative to vehicle treatment, due to the already high baseline T_{IBAT} which likely impeded the ability of 4V OT to further elevate T_{IBAT}. However, when OT was administered into the 4V during the early-light cycle (when baseline T_{IBAT} tends to be lower), 4V OT tended to elevate T_{IBAT} to a greater degree at both 0.75- ($P = 0.019$) and 1-h postadministration ($P = 0.110$).

Study 2C: Effects of Acute 4V OT Administration during Early-Light Cycle on T_{IBAT} in Male DIO Mice

In a separate group of DIO mice (n = 13/group), there was a significant main effect of 4V OT to elevate T_{IBAT} at 0.15- [($F(2,24) = 4.998$, $P < 0.05$], 0.75- [($F(2,24) = 3.687$, $P < 0.05$], 1- [($F(2,24) = 10.947$, $P < 0.01$], and 1.25-h postinjection [($F(2,24) = 3.811$, $P < 0.01$].

We also found a significant effect of time [($F(8,288) = 14.233$, $P < 0.01$] and a significant interactive effect between time and dose [($F(16,288) = 2.819$, $P < 0.01$] across nine time points over the 120-min measurement period.

Specifically, OT (5 μg) produced a significant increase in T_{IBAT} at 1- and 1.25-h postinjection ($P < 0.05$). The high dose also appeared to stimulate T_{IBAT} at 0.75- ($P = 0.085$), 1.5- ($P = 0.059$), and 1.75-h postinjection ($P = 0.091$) although this did not reach significance. The lowest dose (1 μg) stimulated T_{IBAT} at 0.75- and 1-h postinjection ($P < 0.05$; Fig. 10*A*) and also appeared to stimulate 0.25- ($P = 0.062$) and 1.25-h postinjection ($P = 0.080$), although this did not reach significance. Similar findings were apparent when measuring change in T_{IBAT} relative to baseline T_{IBAT} (Fig. 10*B*). There was also a significant main effect of 4V OT to elevate T_{IBAT} when the data were averaged over the 2-h posttreatment period [($F(2,24) = 3.987$, $P < 0.05$]. Specifically, 4V OT at 1 ($P < 0.05$) and 5 μg ($P < 0.05$) produced significant elevations of T_{IBAT}

Table 1. *Plasma measurements following 4V infusions of OT or vehicle in male chow-fed and HFD-fed DIO mice from study 1A*

	Chow		HFD	
4V Treatment	Vehicle	OT	Vehicle	OT
Leptin, ng/mL	3.2 ± 0.3[a]	2.4 ± 0.3[a]	43.9 ± 5.8[b]	26.9 ± 3.4[c]
Insulin, ng/mL	0.6 ± 0.08[a]	0.5 ± 0.06[a]	1.9 ± 0.6[b]	2.0 ± 0.4[b]
FGF-21, pg/mL	247 ± 51.2[a]	150 ± 25.4[a]	1652 ± 296[b]	1052 ± 134[c]
Irisin, μg/mL	6.0 ± 0.2[a,b]	6.5 ± 0.4[b,c]	7.3 ± 0.6[a]	7.9 ± 0.6[a,c]
Adiponectin, μg/mL	15.0 ± 0.6[a]	13.5 ± 0.6[a]	15.4 ± 0.9[a]	13.8 ± 0.7[a]
Blood glucose, mg/dL	187 ± 5.3[a]	187.5 ± 5.1[a]	180 ± 8.5[a]	180 ± 2.0[a]
FFA, mEq/L	0.24 ± 0.02[b]	0.18 ± 0.01[a]	0.17 ± 0.02[a]	0.15 ± 0.01[a]
Total cholesterol, mg/dL	110 ± 3.2[a]	105 ± 3.7[a]	217.6 ± 10.1[b]	206.9 ± 10.4[b]

Data are expressed as means ± SE. Different letters denote significant differences between treatments. DIO, diet-induced obese; FFA, free fatty acids; FGF, fibroblast growth factor-21; HFD, high-fat diet; OT, oxytocin; 4V, fourth ventricular. Shared letters are not significantly different from one another ($P < 0.05$). n = 8–11/group.

when data were averaged over the 2-h posttreatment period (Fig. 10*C*).

DISCUSSION

The goal of the current studies was to determine *1*) whether chronic hindbrain (4V) administration of OT elicits sustained weight loss in a mouse model of diet-induced obesity, *2*) if this effect is associated with reductions of body adiposity and adipocyte size in addition to reduced energy intake, and *3*) if stimulation of hindbrain OTRs is associated with increased BAT thermogenesis and browning of WAT. Our findings indicate that chronic hindbrain (4V) administration of OT reduces HFD consumption at a dose that did not increase intake of kaolin. These effects were associated with reductions of body fat mass, adipocyte size, and plasma leptin concentrations. Furthermore, we determined that hindbrain administration of OT appeared to elevate UCP-1 expression in IWAT of both DIO and chow-fed control mice, suggesting that hindbrain OT signaling may be linked to browning of WAT. We also confirm that hindbrain administration of OT stimulates BAT thermogenesis in mice and that these effects appeared to be more robust when OT was administered during the early-light cycle. Collectively, these findings support the hypothesis that chronic increases of OT signaling within the hindbrain elicits sustained weight loss in DIO mice by reducing energy intake and increasing BAT thermogenesis at a dose that is not associated with visceral illness.

Our finding that chronic hindbrain (4V) administration of OT evokes weight loss in DIO mice consuming a HFD recapitulate our previous findings from our laboratory and others following 3V administration in the DIO mouse model (10, 23, 24) suggesting that OT's effects on hindbrain OTRs contribute to its effects on weight loss. Moreover, these findings are also similar to our previous findings in the rat model (10) suggesting that sustained activation of hindbrain OTRs is sufficient to elicit weight loss in both rats and mice. These findings also extend previous studies that implicate an important role of endogenous OT signaling within the hindbrain in the control of food intake in mice (57). Future studies will be required to determine the extent to which OTRs in specific hindbrain sites [i.e., nucleus of the solitary tract (NST) or raphe pallidus] are necessary for the anti-obesity effects of OT. Specifically, it will be important to address the extent to which site-specific ablation of OTRs in DIO mice and rats *1*) eliminates the effects of chronic 4V OT to reduce body weight, energy intake, and increase EE and *2*) predisposes animals to diet-induced obesity and metabolic abnormalities associated with diet-induced obesity.

To our knowledge, these are the first data which demonstrate that hindbrain administration of OT increases T_{IBAT} in a mouse model. Furthermore, these data also indicate that OT's effects on T_{IBAT} appear to be more robust when it is administered early during the light cycle. Our finding is also consistent with an earlier report in DIO mice that indicate that OT produces a more robust effect on body weight and EE when administered during the early-light cycle relative to later in the light cycle (24). These effects may be attributed, in part, to *1*) the ability of exogenous OT to restore impairments in OT diurnal rhythmicity in DIO mice (24) and *2*) reductions of sympathetic nervous system (SNS) outflow to IBAT during the early-light cycle. Previous studies indicate that *1*) circulating norepinephrine concentrations are higher during the dark cycle relative to light cycle (58), *2*) catecholamine content in IBAT is lower during the light cycle compared with dark cycle in rats (59), *3*) peak glucose uptake into IBAT occurs during the late-light cycle (60), and *4*) peak fatty acid uptake into IBAT tends to occur at onset of dark period (61). Elevated SNS outflow to IBAT toward the late-light cycle could also explain, in part, our observation that IBAT temperature appears to be elevated in vehicle-treated mice during this time. Whether OT requires SNS outflow to IBAT to elicit weight loss is the focus of ongoing investigation.

Our findings are the first to demonstrate that hindbrain administration of OT increases browning of WAT in the mouse model. These findings are consistent with recent data showing that subcutaneous infusion of OT can also reduce subcutaneous fat mass in male and female DIO mice (7). In addition, subcutaneous infusion of OT was found to reduce adipocyte size in subcutaneous fat in *db/db* mice (16) and in IWAT of HFD-fed mice (28). Subcutaneous infusion of OT (125 ng/kg/h or ≈ 66.2 nmol/day) also appeared to increase UCP-1 content in subcutaneous fat of *db/db* mice (16), although the data were not quantified in this study. Similar to our findings, subcutaneous infusion of OT (100 nmol/day) also elevated UCP-1 expression in IWAT but not in EWAT of

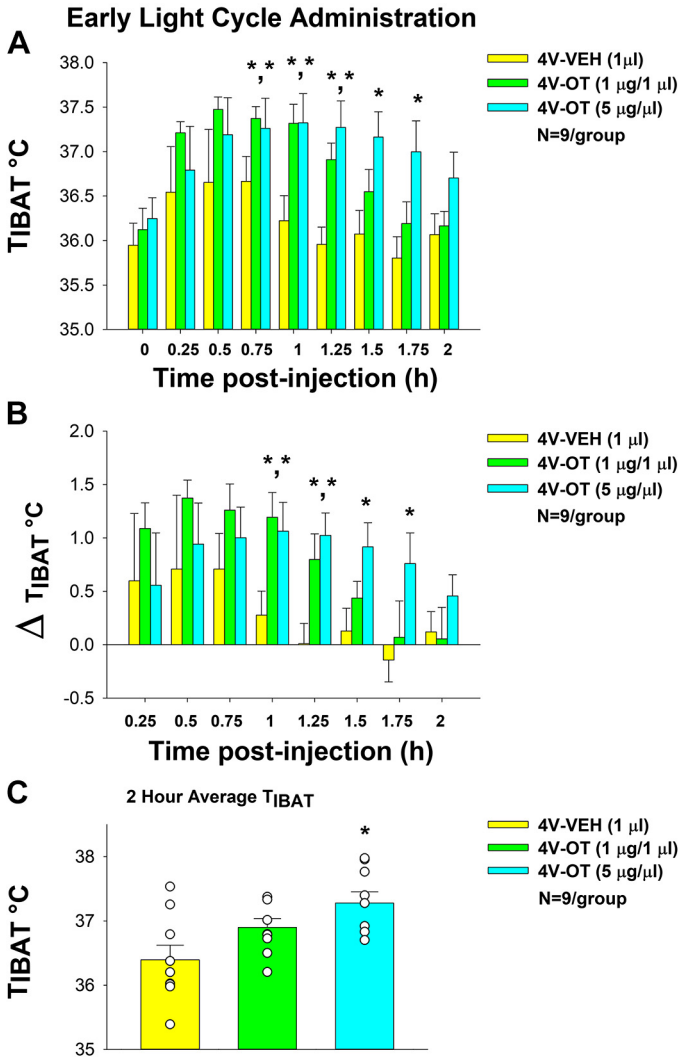

Figure 8. Effects of fourth ventricular (4V) oxytocin (OT) administration during the early-light cycle on interscapular brown adipose tissue (BAT) temperature (T_{IBAT}) in male chow-fed mice. *A*: T_{IBAT} was measured in mice that received acute 4V injections of OT (1, 5 µg/µL) or vehicle (n = 9/group). *B*: change in T_{IBAT} relative to baseline T_{IBAT} was measured in mice that received an acute 4V injection of OT (1, 5 µg/µL) or vehicle (n = 9/group). *C*: 2-h average T_{IBAT} following 4V injection of OT (1, 5 µg/µL) or vehicle. One-way repeated-measures ANOVA; data are expressed as means ± SE. *$P < 0.05$ vs. vehicle.

HFD-fed mice (28). Although it is possible that the effects observed on WAT browning in our study may be attributed, in part, to leakage from the 4V to OTRs in the spinal cord and/or periphery it is important to note that the dose used in the earlier study in DIO mice was ~6.25-fold (28) higher than that found to be effective following hindbrain delivery in the current study. Collectively, these findings suggest that, in addition to a central mechanism mediated through hindbrain and/or spinal cord OTRs, OT may also act peripherally to induce browning of WAT through a direct action on OTRs found on adipocytes (6, 62, 63).

It is not clear why OT elicited differential effects on browning in IWAT and EWAT although it is clear that fat depots may receive anatomically and functionally specific input from the SNS. Bartness and coworkers have found that central administration of MTII, which may act, in part through OT signaling, also elicits differential effects on norepinephrine turnover (NETO; surrogate marker of SNS outflow) across WAT depots. In particular, Brito et al. (39) found that central administration produced differential effects on SNS outflow to WAT and IBAT. In addition, they found that MTII increased NETO to inguinal WAT as well as dorsosubcutaneous WAT and IBAT NETO, but it did not alter NETO in epididymal WAT or retroperitoneal WAT. Given that browning of WAT is dependent on SNS innervation of WAT (64) and that SNS outflow to various WAT (including IWAT and EWAT) can be separate or distinct (65), OT may be eliciting these effects through alterations in SNS outflow in a fat pad specific manner. It remains to be determined if hindbrain OT elicits differential effects on WAT browning, in part, through distinct neuronal projections originating in the NST or raphe pallidus, that are anatomically positioned to

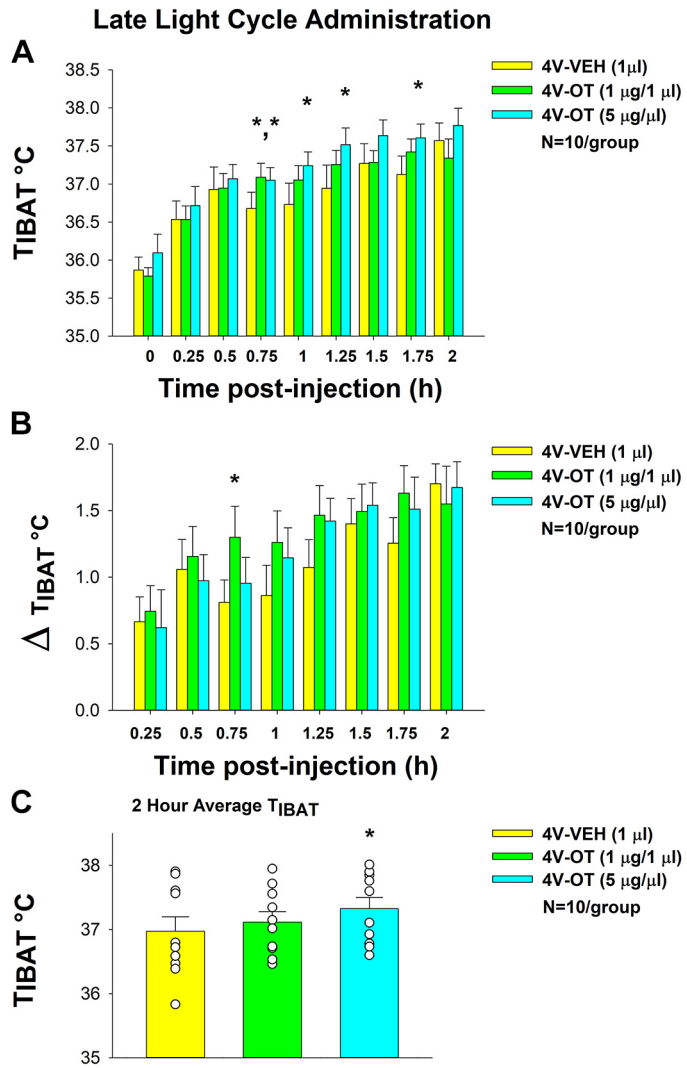

Figure 9. Effects of fourth ventricular (4V) oxytocin (OT) administration during the late-light cycle on interscapular brown adipose tissue (BAT) temperature (T_{IBAT}) in male chow-fed mice. *A*: T_{IBAT} was measured in mice that received acute 4V injections of OT (1, 5 µg/µL) or vehicle (n = 10/group). *B*: change in T_{IBAT} relative to baseline T_{IBAT} was measured in mice that received an acute 4V injection of OT (1, 5 µg/µL) or vehicle (n = 10/group). *C*: 2-h average T_{IBAT} following 4V injection of OT (1, 5 µg/µL) or vehicle. One-way repeated-measures ANOVA; data are expressed as means ± SE. *$P < 0.05$ vs. vehicle.

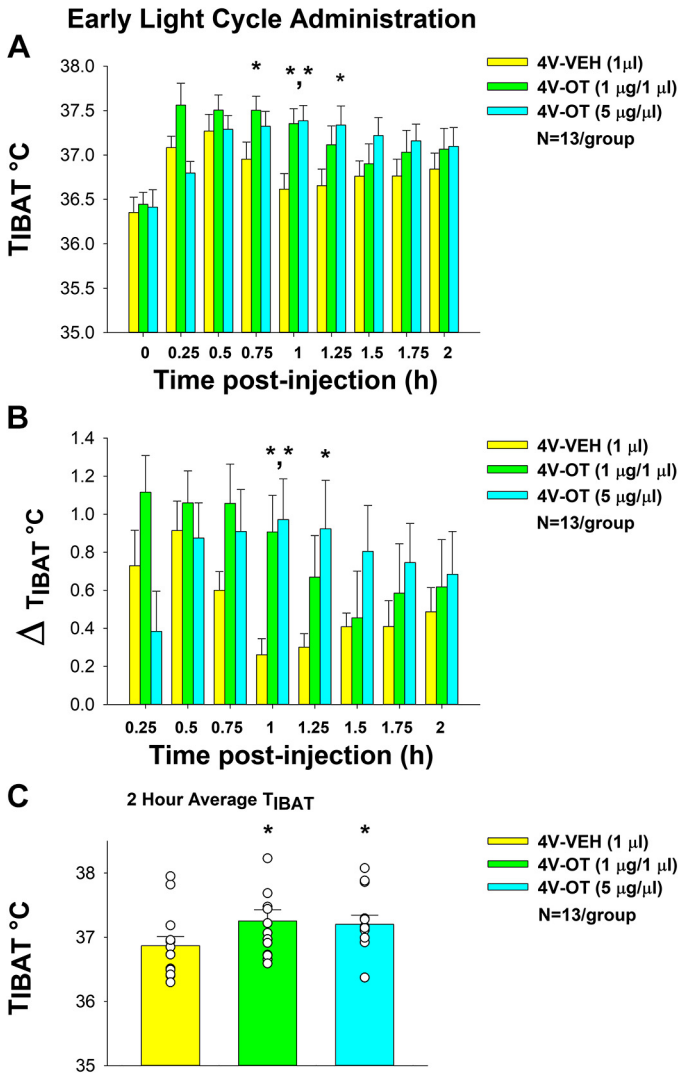

Figure 10. Effects of acute fourth ventricular (4V) oxytocin (OT) administration during early-light cycle on interscapular brown adipose tissue (BAT) temperature (T_{IBAT}) in male diet-induced obese (DIO) mice. *A*: T_{IBAT} was measured in mice that received acute 4V injections of OT (1, 5 µg/µL) or vehicle ($n = 13$/group). *B*: change in T_{IBAT} relative to baseline T_{IBAT} was measured in mice that received an acute 4V injection of OT (1, 5 µg/µL) or vehicle ($n = 10$/group). *C*: two-hour average T_{IBAT} following 4V injection of OT (1, 5 µg/µL) or vehicle. One-way repeated-measures ANOVA; data are expressed as means ± SE. $^*P < 0.05$ vs. vehicle.

regulate SNS outflow to WAT (66–69) and express OTRs [mice: (70, 71)/rats: (72–75)]. Bartness and coworkers (39, 76) had speculated that EWAT may not be as prone to other lipolytic factors such as glucoprivation, fasting, and cold exposure, in part, because removal of this fat depot can negatively impact spermatogenesis (77).

Although our findings do not differentiate a hindbrain from spinal cord site of OT action in the regulation of BAT thermogenesis or browning of WAT, functional and/or anatomical data support both possibilities. Sutton et al. (27) have published recent data to suggest that spinal cord OTRs could be important in the control of BAT thermogenesis and EE in *Oxytocin-Ires-Cre* mice. Recent anatomical data indicate the existence of both shared and separate CNS circuits that control SNS outflow to IBAT and IWAT (78) in Siberian hamsters. In particular, parvocellular PVN (pPVN) OT neuronal cell bodies have been found to project to IBAT (79, 80) (rats), EWAT (67, 69) (Siberian hamsters, rats) and IWAT (67, 79) (Siberian hamsters, rats), and a small subset of PVN OT neurons overlap and project to both IBAT and IWAT (79) (rats). OT neurons are thus anatomically positioned to control SNS outflow to IBAT and IWAT to stimulate BAT thermogenesis and browning of IWAT, respectively. This could occur, in part, through direct descending projections to the hindbrain NST (81, 82) and/or spinal cord (82), both of which may regulate SNS outflow to IBAT and WAT and are linked to the control of BAT thermogenesis (83, 84). Whether OTRs within the NST, other hindbrain areas (including the raphe pallidus) (34, 84–87) or spinal cord (27) contribute to the effects of 4V OT on weight loss as well as BAT thermogenesis and browning of WAT remains to be determined.

Given the heterogeneity with respect to pPVN OT populations and outgoing projections to hindbrain or spinal cord, targeting specific PVN OT neuronal populations or axonal projections will be helpful in differentiating the roles of specific neuronal subsets that control food intake from those that control SNS outflow to IBAT and IWAT to impact EE. Current studies raise the possibility of species differences in the anatomical origin (rostral versus caudal) of the more predominant descending pPVN OT neuronal projections to the hindbrain. Specifically, the pPVN OT neurons that project to the hindbrain NST are primarily located in the caudal pPVN in rats (81). Although it remains to be determined if this is also true in mice, there appear to be few OT projections from the rostral pPVN to the NST in mice and those in the rostral PVN appear to project to spinal cord (27). These findings raise the possibility that parvocellular PVN OT neurons located more caudally project to subsets of NST OTR-expressing neurons in both mice and rats. It is also possible that, in mice, pPVN OT neurons do not innervate the hindbrain as heavily relative to rats, although studies provide indirect evidence in support of such a projection in mice (57, 88–90) and suggest that caudal hindbrain OTR are important in the control of energy balance in both mice (57, 88) and rats (72–74, 91, 92).

Our findings raise the possibility that increased locomotor activity may contribute, in part, to the elevated IBAT temperature in these animals. Others have found that DREADD-elicited activation of PVN oxytocin neurons in *Oxytocin-IRES-Cre* mice resulted in a small increase in locomotor activity, energy expenditure and subcutaneous IBAT temperature (27) in animals whose transponders were placed above the IBAT pad. One study did show that acute OT administration into the ventromedial hypothalamus increased physical activity in the rat model at 1-h postinjection (REF) but these effects failed to match the more extended effects of OT on T_{IBAT} that we have found following CNS administration in rats (10) and mice (10). We and others have also found that chronic lateral ventricular or third ventricular (3 V) OT, at a dose that reduces body weight and elevates T_{IBAT}, did not impact locomotor activity in DIO rats (6, 10, 17). Maejima et al. (8) have also demonstrated that systemic administration of OT also failed to impact locomotor activity at a dose that reduced body weight in DIO mice. In addition, Carson et al. (93) found that systemic administration of OT reduced methamphetamine-elicited elevations in locomotor activity in

rats. Furthermore, systemic OT reduced locomotor activity in rats and this effect was blocked following central administration of an OTR antagonist (94). In addition, central delivery of OT was found to block the effects of central administration of an OTR antagonist to increase locomotor activity. Although the majority of studies suggest that OT either has no impact or reduces locomotor activity, future studies will be required in order to examine the extent to which locomotor activity may contribute to the effects of acute 4V on both T_{IBAT}.

Perspectives and Significance

Obesity is a growing health concern and increases the risk for heart disease, hypertension, type 2 diabetes (T2D), cancer, and overall morbidity and mortality, including that from COVID-19 infection (95–100). Obesity rates have reached epidemic proportions in the US and worldwide. According to the National Center for Health Statistics, obesity prevalence (age-adjusted) between 1999–2000 and 2017–2018 has increased in adults from 30.5% to 42.4% (101). Nearly 73 million people in the United States alone are considered overweight or obese (102, 103) and the projected health care costs to treat the medical consequences of obesity is 147 billion dollars (104). In addition to these alarming statistics, current anti-obesity medications are often poorly tolerated and associated with adverse side effects [including nausea and insomnia (105)], thus highlighting the need for new and more effective treatments.

Our findings demonstrate that hindbrain OT administration reduces energy intake and increases BAT thermogenesis leading to the reduction of body weight and fat mass without eliciting a reduction in lean mass in a mouse model. Moreover, these effects were not associated with increased consumption of kaolin suggesting that hindbrain OT treatment is not associated with visceral illness in our mouse model. In addition, they confirm that optimal effects for OT delivery may be achieved when OT is administered during the early- to mid-light cycle which is consistent with the recent findings from Zhang and Cai (24). It will be important to address the extent to which OT-elicited activation of SNS outflow to BAT is required for OT to elicit weight loss. Given the positive findings in male DIO mice and the recently reported anti-obesogenic effects in response to systemic OT treatment in female DIO mice (7), future studies should also address the extent to which hindbrain administration reduces body weight and adiposity in female DIO mice.

ACKNOWLEDGMENTS

The authors thank the technical support of Nishi Ivanov, Zachary Roberts, Miles Matsen, Hailey Chadwick, and Alex Vu. In addition, the authors are appreciative of the efforts by Drs. Gerald Taborsky, Jr., Michael Schwartz, and Gregory Morton for providing feedback throughout these studies.

GRANTS

This material was based upon work supported by the Office of Research and Development, Medical Research Service, Department of Veterans Affairs (VA) and the VA Puget Sound Health Care System Rodent Metabolic Phenotyping Core, and the Cellular and Molecular Imaging Core of the Diabetes Research Center at the University of Washington and supported by National Institutes of Health (NIH) Grant P30DK017047. This work was also supported by the VA Merit Review Award 5I01BX004102, from the US Department of Veterans Affairs Biomedical Laboratory Research and Development Service and NIH 5R01DK115976 Grant to J. E. Blevins. P. J. Havel's research program also received research support during the project period from NIH Grants DK-095980, HL-091333, and HL-107256 and a Multi-campus Grant from the University of California Office of the President.

DISCLAIMERS

The contents do not represent the views of the US Department of Veterans Affairs or the US Government.

DISCLOSURES

J.E.B. has a financial interest in OXT Therapeutics, Inc., a company developing highly specific and stable analogs of oxytocin to treat obesity and metabolic disease. The authors' interests were reviewed and are managed by their local institutions in accordance with their conflict of interest policies. None of the other authors has any conflicts of interest, financial or otherwise, to disclose.

AUTHOR CONTRIBUTIONS

J.E.B. conceived and designed research; M.M.E., H.K.N., A.J.H., A.D.D., T.W., T.W-H., J.L.G., and J.E.B. performed experiments; T.W., T.W-H., J.L.G., and J.E.B., analyzed data; T.W., T.W-H., J.L.G., and J.E.B. interpreted results of experiments; J.E.B. prepared figures; M.M.E., H.K.N., T.W., J.L.G., P.J.H., and J.E.B. drafted manuscript; M.M.E., H.K.N., A.J.H., A.D.D., T.W., T.W-H., J.L.G., K.D.O., P.J.H., and J.E.B. edited and revised manuscript; M.M.E., H.K.N., A.J.H., A.D.D., T.W., T.W-H., J.L.G., K.D.O., P.J.H., and J.E.B. approved final version of manuscript.

REFERENCES

1. **Blevins JE**, **Baskin DG.** Translational and therapeutic potential of oxytocin as an anti-obesity strategy: insights from rodents, nonhuman primates and humans. *Physiol Behav* 152: 438–439, 2015. doi:10.1016/j.physbeh.2015.05.023.
2. **Lawson EA.** The effects of oxytocin on eating behaviour and metabolism in humans. *Nat Rev Endocrinol* 13: 700–709, 2017. doi:10.1038/nrendo.2017.115.
3. **Lawson EA**, **Olszewski PK**, **Weller A**, **Blevins JE.** The role of oxytocin in regulation of appetitive behaviour, body weight and glucose homeostasis. *J Neuroendocrinol* 32: e12805, 2020. doi:10.1111/jne.12805.
4. **McCormack SE**, **Blevins JE**, **Lawson EA.** Metabolic effects of oxytocin. *Endocr Rev* 41: 121–145, 2020. doi:10.1210/endrev/bnz012.
5. **Blevins JE**, **Thompson BW**, **Anekonda VT**, **Ho JM**, **Graham JL**, **Roberts ZS**, **Hwang BH**, **Ogimoto K**, **Wolden-Hanson TH**, **Nelson JO**, **Kaiyala KJ**, **Havel PJ**, **Bales KL**, **Morton GJ**, **Schwartz MW**, **Baskin DG.** Chronic CNS oxytocin signaling preferentially induces fat loss in high fat diet-fed rats by enhancing satiety responses and increasing lipid utilization. *Am J Physiol Regul Integr Comp Physiol* 310: R640–R658, 2016. doi:10.1152/ajpregu.00220.2015.
6. **Deblon N**, **Veyrat-Durebex C**, **Bourgoin L**, **Caillon A**, **Bussier AL**, **Petrosino S**, **Piscitelli F**, **Legros JJ**, **Geenen V**, **Foti M**, **Wahli W**, **Di Marzo V**, **Rohner-Jeanrenaud F.** Mechanisms of the anti-obesity effects of oxytocin in diet-induced obese rats. *PLoS One* 6: e25565, 2011. doi:10.1371/journal.pone.0025565.
7. **Maejima Y**, **Aoyama M**, **Sakamoto K**, **Jojima T**, **Aso Y**, **Takasu K**, **Takenosihita S**, **Shimomura K.** Impact of sex, fat distribution and initial body weight on oxytocin's body weight regulation. *Sci Rep* 7: 8599, 2017. doi:10.1038/s41598-017-09318-7.

8. **Maejima Y**, **Iwasaki Y**, **Yamahara Y**, **Kodaira M**, **Sedbazar U**, **Yada T.** Peripheral oxytocin treatment ameliorates obesity by reducing food intake and visceral fat mass. *Aging (Albany NY)* 3: 1169–1177, 2011. doi:10.18632/aging.100408.
9. **Morton GJ**, **Thatcher BS**, **Reidelberger RD**, **Ogimoto K**, **Wolden-Hanson T**, **Baskin DG**, **Schwartz MW**, **Blevins JE.** Peripheral oxytocin suppresses food intake and causes weight loss in diet-induced obese rats. *Am J Physiol Endocrinol Metab* 302: E134–E144, 2012. doi:10.1152/ajpendo.00296.2011.
10. **Roberts ZS**, **Wolden-Hanson TH**, **Matsen ME**, **Ryu V**, **Vaughan CH**, **Graham JL**, **Havel PJ**, **Chukri DW**, **Schwartz MW**, **Morton GJ**, **Blevins JE.** Chronic hindbrain administration of oxytocin is sufficient to elicit weight loss in diet-induced obese rats. *Am J Physiol Regul Integr Comp Physiol* 313: R357–R371, 2017. doi:10.1152/ajpregu.00169.2017.
11. **Altirriba J**, **Poher AL**, **Rohner-Jeanrenaud F.** Chronic oxytocin administration as a treatment against impaired leptin signaling or leptin resistance in obesity. *Front Endocrinol (Lausanne)* 6: 119, 2015. doi:10.3389/fendo.2015.00119.
12. **Balazova L**, **Krskova K**, **Suski M**, **Sisovsky V**, **Hlavacova N**, **Olszanecki R**, **Jezova D**, **Zorad S.** Metabolic effects of subchronic peripheral oxytocin administration in lean and obese zucker rats. *J Physiol Pharmacol* 67: 531–541, 2016.
13. **Iwasaki Y**, **Maejima Y**, **Suyama S**, **Yoshida M**, **Arai T**, **Katsurada K**, **Kumari P**, **Nakabayashi H**, **Kakei M**, **Yada T.** Peripheral oxytocin activates vagal afferent neurons to suppress feeding in normal and leptin-resistant mice: a route for ameliorating hyperphagia and obesity. *Am J Physiol Regul Integr Comp Physiol* 308: R360–R369, 2015. doi:10.1152/ajpregu.00344.2014.
14. **Kublaoui BM**, **Gemelli T**, **Tolson KP**, **Wang Y**, **Zinn AR.** Oxytocin deficiency mediates hyperphagic obesity of Sim1 haploinsufficient mice. *Mol Endocrinol* 22: 1723–1734, 2008. doi:10.1210/me.2008-0067.
15. **Maejima Y**, **Sedbazar U**, **Suyama S**, **Kohno D**, **Onaka T**, **Takano E**, **Yoshida N**, **Koike M**, **Uchiyama Y**, **Fujiwara K**, **Yashiro T**, **Horvath TL**, **Dietrich MO**, **Tanaka S**, **Dezaki K**, **Oh IS**, **Hashimoto K**, **Shimizu H**, **Nakata M**, **Mori M**, **Yada T.** Nesfatin-1-regulated oxytocinergic signaling in the paraventricular nucleus causes anorexia through a leptin-independent melanocortin pathway. *Cell Metab* 10: 355–365, 2009. doi:10.1016/j.cmet.2009.09.002.
16. **Plante E**, **Menaouar A**, **Danalache BA**, **Yip D**, **Broderick TL**, **Chiasson JL**, **Jankowski M**, **Gutkowska J.** Oxytocin treatment prevents the cardiomyopathy observed in obese diabetic male db/db mice. *Endocrinology* 156: 1416–1428, 2015. doi:10.1210/en.2014-1718.
17. **Blevins JE**, **Graham JL**, **Morton GJ**, **Bales KL**, **Schwartz MW**, **Baskin DG**, **Havel PJ.** Chronic oxytocin administration inhibits food intake, increases energy expenditure, and produces weight loss in fructose-fed obese rhesus monkeys. *Am J Physiol Regul Integr Comp Physiol* 308: R431–R438, 2015. doi:10.1152/ajpregu.00441.2014.
18. **Lawson EA**, **Marengi DA**, **DeSanti RL**, **Holmes TM**, **Schoenfeld DA**, **Tolley CJ.** Oxytocin reduces caloric intake in men. *Obesity (Silver Spring)* 23: 950–956, 2015. doi:10.1002/oby.21069.
19. **Spetter MS**, **Feld GB**, **Thienel M**, **Preissl H**, **Hege MA**, **Hallschmid M.** Oxytocin curbs calorie intake via food-specific increases in the activity of brain areas that process reward and establish cognitive control. *Sci Rep* 8: 2736, 2018. doi:10.1038/s41598-018-20963-4.
20. **Thienel M**, **Fritsche A**, **Heinrichs M**, **Peter A**, **Ewers M**, **Lehnert H**, **Born J**, **Hallschmid M.** Oxytocin's inhibitory effect on food intake is stronger in obese than normal-weight men. *Int J Obes (Lond)* 40: 1707–1714, 2016. doi:10.1038/ijo.2016.149.
21. **Zhang H**, **Wu C**, **Chen Q**, **Chen X**, **Xu Z**, **Wu J**, **Cai D.** Treatment of obesity and diabetes using oxytocin or analogs in patients and mouse models. *PLoS One* 8: e61477, 2013. doi:10.1371/journal.pone.0061477.
22. **Altirriba J**, **Poher AL**, **Caillon A**, **Arsenijevic D**, **Veyrat-Durebex C**, **Lyautey J**, **Dulloo A**, **Rohner-Jeanrenaud F.** Divergent effects of oxytocin treatment of obese diabetic mice on adiposity and diabetes. *Endocrinology* 155: 4189–4201, 2014. doi:10.1210/en.2014-1466.
23. **Zhang G**, **Bai H**, **Zhang H**, **Dean C**, **Wu Q**, **Li J**, **Guariglia S**, **Meng Q**, **Cai D.** Neuropeptide exocytosis involving synaptotagmin-4 and oxytocin in hypothalamic programming of body weight and energy balance. *Neuron* 69: 523–535, 2011. doi:10.1016/j.neuron.2010.12.036.
24. **Zhang G**, **Cai D.** Circadian intervention of obesity development via resting-stage feeding manipulation or oxytocin treatment. *Am J Physiol Endocrinol Metab* 301: E1004–E1012, 2011. doi:10.1152/ajpendo.00196.2011.
25. **Cannon B**, **Nedergaard J.** Brown adipose tissue: function and physiological significance. *Physiol Rev* 84: 277–359, 2004. doi:10.1152/physrev.00015.2003.
26. **Morrison SF**, **Madden CJ**, **Tupone D.** Central neural regulation of brown adipose tissue thermogenesis and energy expenditure. *Cell Metab* 19: 741–756, 2014. doi:10.1016/j.cmet.2014.02.007.
27. **Sutton AK**, **Pei H**, **Burnett KH**, **Myers MG Jr**, **Rhodes CJ**, **Olson DP.** Control of food intake and energy expenditure by Nos1 neurons of the paraventricular hypothalamus. *J Neurosci* 34: 15306–15318, 2014. doi:10.1523/JNEUROSCI.0226-14.2014.
28. **Yuan J**, **Zhang R**, **Wu R**, **Gu Y**, **Lu Y.** The effects of oxytocin to rectify metabolic dysfunction in obese mice are associated with increased thermogenesis. *Mol Cell Endocrinol* 514: 110903, 2020. doi:10.1016/j.mce.2020.110903.
29. **Camerino C.** Low sympathetic tone and obese phenotype in oxytocin-deficient mice. *Obesity (Silver Spring)* 17: 980–984, 2009. doi:10.1038/oby.2009.12.
30. **Takayanagi Y**, **Kasahara Y**, **Onaka T**, **Takahashi N**, **Kawada T**, **Nishimori K.** Oxytocin receptor-deficient mice developed late-onset obesity. *Neuroreport* 19: 951–955, 2008. doi:10.1097/WNR.0b013e3283021ca9.
31. **Wu Z**, **Xu Y**, **Zhu Y**, **Sutton AK**, **Zhao R**, **Lowell BB**, **Olson DP**, **Tong Q.** An obligate role of oxytocin neurons in diet induced energy expenditure. *PLoS One* 7: e45167, 2012. doi:10.1371/journal.pone.0045167.
32. **Kasahara Y**, **Sato K**, **Takayanagi Y**, **Mizukami H**, **Ozawa K**, **Hidema S**, **So KH**, **Kawada T**, **Inoue N**, **Ikeda I**, **Roh SG**, **Itoi K**, **Nishimori K.** Oxytocin receptor in the hypothalamus is sufficient to rescue normal thermoregulatory function in male oxytocin receptor knockout mice. *Endocrinology* 154: 4305–4315, 2013. doi:10.1210/en.2012-2206.
33. **Harshaw C**, **Leffel JK**, **Alberts JR.** Oxytocin and the warm outer glow: thermoregulatory deficits cause huddling abnormalities in oxytocin-deficient mouse pups. *Horm Behav* 98: 145–158, 2018. doi:10.1016/j.yhbeh.2017.12.007.
34. **Kasahara Y**, **Tateishi Y**, **Hiraoka Y**, **Otsuka A**, **Mizukami H**, **Ozawa K**, **Sato K**, **Hidema S**, **Nishimori K.** Role of the oxytocin receptor expressed in the rostral medullary raphe in thermoregulation during cold conditions. *Front Endocrinol (Lausanne)* 6: 180, 2015. doi:10.3389/fendo.2015.00180.
35. **Xi D**, **Long C**, **Lai M**, **Casella A**, **O'Lear L**, **Kublaoui B**, **Roizen JD.** Ablation of oxytocin neurons causes a deficit in cold stress response. *J Endocr Soc* 1: 1041–1055, 2017. doi:10.1210/js.2017-00136.
36. **Blevins JE**, **Schwartz MW**, **Baskin DG.** Evidence that paraventricular nucleus oxytocin neurons link hypothalamic leptin action to caudal brain stem nuclei controlling meal size. *Am J Physiol Regul Integr Comp Physiol* 287: R87–R96, 2004. doi:10.1152/ajpregu.00604.2003.
37. **Morton GJ**, **Matsen ME**, **Bracy DP**, **Meek TH**, **Nguyen HT**, **Stefanovski D**, **Bergman RN**, **Wasserman DH**, **Schwartz MW.** FGF19 action in the brain induces insulin-independent glucose lowering. *J Clin Invest* 123: 4799–4808, 2013. doi:10.1172/JCI70710.
38. **Dorfman MD**, **Krull JE**, **Douglass JD**, **Fasnacht R**, **Lara-Lince F**, **Meek TH**, **Shi X**, **Damian V**, **Nguyen HT**, **Matsen ME**, **Morton GJ**, **Thaler JP.** Sex differences in microglial CX3CR1 signalling determine obesity susceptibility in mice. *Nat Commun* 8: 14556, 2017. doi:10.1038/ncomms14556.
39. **Brito MN**, **Brito NA**, **Baro DJ**, **Song CK**, **Bartness TJ.** Differential activation of the sympathetic innervation of adipose tissues by melanocortin receptor stimulation. *Endocrinology* 148: 5339–5347, 2007. doi:10.1210/en.2007-0621.
40. **Vaughan CH**, **Shrestha YB**, **Bartness TJ.** Characterization of a novel melanocortin receptor-containing node in the SNS outflow circuitry to brown adipose tissue involved in thermogenesis. *Brain Res* 1411: 17–27, 2011. doi:10.1016/j.brainres.2011.07.003.
41. **den Hartigh LJ**, **Wang SR**, **Goodspeed L**, **Wietecha T**, **Houston B**, **Omer M**, **Ogimoto K**, **Subramanian S**, **Gowda GAN**, **O'Brien KD**, **Kaiyala KJ**, **Morton GJ**, **Chait A.** Metabolically distinct weight loss by 10,12 CLA and caloric restriction highlight the importance of subcutaneous white adipose tissue for glucose homeostasis in mice. *PLoS One* 12: e0172912, 2017. doi:10.1371/journal.pone.0172912.

42. **Yin N**, **Zhang H**, **Ye R**, **Dong M**, **Lin J**, **Zhou H**, **Huang Y**, **Chen L**, **Jiang X**, **Nagaoka K**, **Zhang C**, **Jin W.** Fluvastatin sodium ameliorates obesity through brown fat activation. *Int J Mol Sci* 20: 1622, 2019. doi:10.3390/ijms20071622.
43. **Chan CB**, **Tse MC**, **Liu X**, **Zhang S**, **Schmidt R**, **Otten R**, **Liu L**, **Ye K.** Activation of muscular TrkB by its small molecular agonist 7,8-dihydroxyflavone sex-dependently regulates energy metabolism in diet-induced obese mice. *Chem Biol* 22: 355–368, 2015. doi:10.1016/j.chembiol.2015.02.003.
44. **Bremer AA**, **Stanhope KL**, **Graham JL**, **Cummings BP**, **Wang W**, **Saville BR**, **Havel PJ.** Fructose-fed rhesus monkeys: a nonhuman primate model of insulin resistance, metabolic syndrome, and type 2 diabetes. *Clin Transl Sci* 4: 243–252, 2011. doi:10.1111/j.1752-8062.2011.00298.x.
45. **Blevins JE**, **Moralejo DH**, **Wolden-Hanson TH**, **Thatcher BS**, **Ho JM**, **Kaiyala KJ**, **Matsumoto K.** Alterations in activity and energy expenditure contribute to lean phenotype in Fischer 344 rats lacking the cholecystokinin-1 receptor gene. *Am J Physiol Regul Integr Comp Physiol* 303: R1231–R1240, 2012. doi:10.1152/ajpregu.00393.2012.
46. **Cummings BP**, **Digitale EK**, **Stanhope KL**, **Graham JL**, **Baskin DG**, **Reed BJ**, **Sweet IR**, **Griffen SC**, **Havel PJ.** Development and characterization of a novel rat model of type 2 diabetes mellitus: the UC Davis type 2 diabetes mellitus UCD-T2DM rat. *Am J Physiol Regul Integr Comp Physiol* 295: R1782–R1793, 2008. doi:10.1152/ajpregu.90635.2008.
47. **Blevins JE**, **Stanley BG**, **Reidelberger RD.** Brain regions where cholecystokinin suppresses feeding in rats. *Brain Res* 860: 1–10, 2000. doi:10.1016/S0006-8993(99)02477-4.
48. **Blevins JE**, **Stanley BG**, **Reidelberger RD.** DMSO as a vehicle for central injections: tests with feeding elicited by norepinephrine injected into the paraventricular nucleus. *Pharmacol Biochem Behav* 71: 277–282, 2002. doi:10.1016/S0091-3057(01)00659-1.
49. **Blevins JE**, **Teh PS**, **Wang CX**, **Gietzen DW.** Effects of amino acid deficiency on monoamines in the lateral hypothalamus (LH) in rats. *Nutr Neurosci* 6: 291–299, 2003. doi:10.1080/1028415031000162248.
50. **Blevins JE**, **Truong BG**, **Gietzen DW.** NMDA receptor function within the anterior piriform cortex and lateral hypothalamus in rats on the control of intake of amino acid-deficient diets. *Brain Res* 1019: 124–133, 2004. doi:10.1016/j.brainres.2004.05.089.
51. **De Jonghe BC**, **Holland RA**, **Olivos DR**, **Rupprecht LE**, **Kanoski SE**, **Hayes MR.** Hindbrain GLP-1 receptor mediation of cisplatin-induced anorexia and nausea. *Physiol Behav* 153: 109–114, 2016. doi:10.1016/j.physbeh.2015.10.031.
52. **Mitchell D**, **Krusemark ML**, **Hafner D.** Pica: a species relevant behavioral assay of motion sickness in the rat. *Physiol Behav* 18: 125–130, 1977. doi:10.1016/0031-9384(77)90103-2.
53. **Mitchell D**, **Winter W**, **Morisaki CM.** Conditioned taste aversions accompanied by geophagia: evidence for the occurrence of "psychological" factors in the etiology of pica. *Psychosom Med* 39: 401–412, 1977.
54. **Seeley RJ**, **Blake K**, **Rushing PA**, **Benoit S**, **Eng J**, **Woods SC**, **D'Alessio D.** The role of CNS glucagon-like peptide-1 (7-36) amide receptors in mediating the visceral illness effects of lithium chloride. *J Neurosci* 20: 1616–1621, 2000. doi:10.1523/JNEUROSCI.20-04-01616.2000.
55. **Yamamoto K**, **Yamatodani A.** Strain differences in the development of cisplatin-induced pica behavior in mice. *J Pharmacol Toxicol Methods* 91: 66–71, 2018. doi:10.1016/j.vascn.2018.01.559.
56. **Noble EE**, **Billington CJ**, **Kotz CM**, **Wang C.** Oxytocin in the ventromedial hypothalamic nucleus reduces feeding and acutely increases energy expenditure. *Am J Physiol Regul Integr Comp Physiol* 307: R737–R745, 2014. doi:10.1152/ajpregu.00118.2014.
57. **Blouet C**, **Jo YH**, **Li X**, **Schwartz GJ.** Mediobasal hypothalamic leucine sensing regulates food intake through activation of a hypothalamus-brainstem circuit. *J Neurosci* 29: 8302–8311, 2009. doi:10.1523/JNEUROSCI.1668-09.2009.
58. **De Boer SF**, **Van der Gugten J.** Daily variations in plasma noradrenaline, adrenaline and corticosterone concentrations in rats. *Physiol Behav* 40: 323–328, 1987. doi:10.1016/0031-9384(87)90054-0.
59. **Davidovic V**, **Petrovic VM.** Diurnal variations in the catecholamine content in rat tissues. Effects of exogenous noradrenaline. *Arch Int Physiol Biochim* 89: 457–460, 1981. doi:10.3109/13813458109082642.
60. **van der Veen DR**, **Shao J**, **Chapman S**, **Leevy WM**, **Duffield GE.** A diurnal rhythm in glucose uptake in brown adipose tissue revealed by in vivo PET-FDG imaging. *Obesity (Silver Spring)* 20: 1527–1529, 2012. doi:10.1038/oby.2012.78.
61. **van den Berg R**, **Kooijman S**, **Noordam R**, **Ramkisoensing A**, **Abreu-Vieira G**, **Tambyrajah LL**, **Dijk W**, **Ruppert P**, **Mol IM**, **Kramar B**, **Caputo R**, **Puig LS**, **de Ruiter EM**, **Kroon J**, **Hoekstra M**, **van der Sluis RJ**, **Meijer OC**, **Willems van Dijk K**, **van Kerkhof LWM**, **Christodoulides C**, **Karpe F**, **Gerhart-Hines Z**, **Kersten S**, **Meijer JH**, **Coomans CP**, **van Heemst D**, **Biermasz NR**, **Rensen PCN.** A diurnal rhythm in brown adipose tissue causes rapid clearance and combustion of plasma lipids at wakening. *Cell Rep* 22: 3521–3533, 2018. doi:10.1016/j.celrep.2018.03.004.
62. **Schaffler A**, **Binart N**, **Scholmerich J**, **Buchler C.** Hypothesis paper Brain talks with fat—evidence for a hypothalamic-pituitary-adipose axis? *Neuropeptides* 39: 363–367, 2005. doi:10.1016/j.npep.2005.06.003.
63. **Yi KJ**, **So KH**, **Hata Y**, **Suzuki Y**, **Kato D**, **Watanabe K**, **Aso H**, **Kasahara Y**, **Nishimori K**, **Chen C**, **Katoh K**, **Roh SG.** The regulation of oxytocin receptor gene expression during adipogenesis. *J Neuroendocrinol* 27: 335–342, 2015. doi:10.1111/jne.12268.
64. **Cao Q**, **Jing J**, **Cui X**, **Shi H**, **Xue B.** Sympathetic nerve innervation is required for beigeing in white fat. *Physiol Rep* 7: e14031, 2019 [Erratum in *Physiol Rep* 7: e14204, 2019]. doi:10.14814/phy2.14031.
65. **Youngstrom TG**, **Bartness TJ.** Catecholaminergic innervation of white adipose tissue in Siberian hamsters. *Am J Physiol* 268: R744–R751, 1995. doi:10.1152/ajpregu.1995.268.3.R744.
66. **Adler ES**, **Hollis JH**, **Clarke IJ**, **Grattan DR**, **Oldfield BJ.** Neurochemical characterization and sexual dimorphism of projections from the brain to abdominal and subcutaneous white adipose tissue in the rat. *J Neurosci* 32: 15913–15921, 2012. doi:10.1523/JNEUROSCI.2591-12.2012.
67. **Shi H**, **Bartness TJ.** Neurochemical phenotype of sympathetic nervous system outflow from brain to white fat. *Brain Res Bull* 54: 375–385, 2001. doi:10.1016/S0361-9230(00)00455-X.
68. **Song CK**, **Schwartz GJ**, **Bartness TJ.** Anterograde transneuronal viral tract tracing reveals central sensory circuits from white adipose tissue. *Am J Physiol Regul Integr Comp Physiol* 296: R501–R511, 2009. doi:10.1152/ajpregu.90786.2008.
69. **Stanley S**, **Pinto S**, **Segal J**, **Perez CA**, **Viale A**, **DeFalco J**, **Cai X**, **Heisler LK**, **Friedman JM.** Identification of neuronal subpopulations that project from hypothalamus to both liver and adipose tissue polysynaptically. *Proc Natl Acad Sci USA* 107: 7024–7029, 2010. doi:10.1073/pnas.1002790107.
70. **Gould BR**, **Zingg HH.** Mapping oxytocin receptor gene expression in the mouse brain and mammary gland using an oxytocin receptor-LacZ reporter mouse. *Neuroscience* 122: 155–167, 2003. doi:10.1016/S0306-4522(03)00283-5.
71. **Yoshida M**, **Takayanagi Y**, **Inoue K**, **Kimura T**, **Young LJ**, **Onaka T**, **Nishimori K.** Evidence that oxytocin exerts anxiolytic effects via oxytocin receptor expressed in serotonergic neurons in mice. *J Neurosci* 29: 2259–2271, 2009. doi:10.1523/JNEUROSCI.5593-08.2009.
72. **Baskin DG**, **Kim F**, **Gelling RW**, **Russell BJ**, **Schwartz MW**, **Morton GJ**, **Simhan HN**, **Moralejo DH**, **Blevins JE.** A new oxytocin-saporin cytotoxin for lesioning oxytocin-receptive neurons in the rat hindbrain. *Endocrinology* 151: 4207–4213, 2010. doi:10.1210/en.2010-0295.
73. **Ong ZY**, **Alhadeff AL**, **Grill HJ.** Medial nucleus tractus solitarius oxytocin receptor signaling and food intake control: the role of gastrointestinal satiation signal processing. *Am J Physiol Regul Integr Comp Physiol* 308: R800–R806, 2015. doi:10.1152/ajpregu.00534.2014.
74. **Ong ZY**, **Bongiorno DM**, **Hernando MA**, **Grill HJ.** Effects of endogenous oxytocin receptor signaling in nucleus tractus solitarius on satiation-mediated feeding and thermogenic control in male rats. *Endocrinology* 158: 2826–2836, 2017. doi:10.1210/en.2017-00200.
75. **Verbalis JG**, **Blackburn RE**, **Hoffman GE**, **Stricker EM.** Establishing behavioral and physiological functions of central oxytocin: insights from studies of oxytocin and ingestive behaviors. *Adv Exp Med Biol* 395: 209–225, 1995.
76. **Brito NA**, **Brito MN**, **Bartness TJ.** Differential sympathetic drive to adipose tissues after food deprivation, cold exposure or glucoprivation. *Am J Physiol Regul Integr Comp Physiol* 294: R1445–R1452, 2008. doi:10.1152/ajpregu.00068.2008.

77. **Srinivasan V**, **Thombre DP**, **Lakshmanan S**, **Chakrabarty AS.** Effect of removal of epididymal fat on spermatogenesis in albino rats. *Indian J Exp Biol* 24: 487–488, 1986.
78. **Nguyen NL**, **Barr CL**, **Ryu V**, **Cao Q**, **Xue B**, **Bartness TJ.** Separate and shared sympathetic outflow to white and brown fat coordinately regulate thermoregulation and beige adipocyte recruitment. *Am J Physiol Regul Integr Comp Physiol* 312: R132–R145, 2017. doi:10.1152/ajpregu.00344.2016.
79. **Doslikova B**, **Tchir D**, **McKinty A**, **Zhu X**, **Marks DL**, **Baracos VE**, **Colmers WF.** Convergent neuronal projections from paraventricular nucleus, parabrachial nucleus, and brainstem onto gastrocnemius muscle, white and brown adipose tissue in male rats. *J Comp Neurol* 527: 2826–2842, 2019. doi:10.1002/cne.24710.
80. **Oldfield BJ**, **Giles ME**, **Watson A**, **Anderson C**, **Colvill LM**, **McKinley MJ.** The neurochemical characterisation of hypothalamic pathways projecting polysynaptically to brown adipose tissue in the rat. *Neuroscience* 110: 515–526, 2002. doi:10.1016/S0306-4522(01)00555-3.
81. **Rinaman L.** Oxytocinergic inputs to the nucleus of the solitary tract and dorsal motor nucleus of the vagus in neonatal rats. *J Comp Neurol* 399: 101–109, 1998. doi:10.1002/(sici)1096-9861(19980914)399:1<101::aid-cne8>3.0.co;2-5.
82. **Sawchenko PE**, **Swanson LW.** Immunohistochemical identification of neurons in the paraventricular nucleus of the hypothalamus that project to the medulla or to the spinal cord in the rat. *J Comp Neurol* 205: 260–272, 1982. doi:10.1002/cne.902050306.
83. **Bamshad M**, **Song CK**, **Bartness TJ.** CNS origins of the sympathetic nervous system outflow to brown adipose tissue. *Am J Physiol Regul Integr Comp Physiol* 276: R1569–R1578, 1999. doi:10.1152/ajpregu.1999.276.6.R1569.
84. **Cano G**, **Passerin AM**, **Schiltz JC**, **Card JP**, **Morrison SF**, **Sved AF.** Anatomical substrates for the central control of sympathetic outflow to interscapular adipose tissue during cold exposure. *J Comp Neurol* 460: 303–326, 2003. doi:10.1002/cne.10643.
85. **Kong D**, **Tong Q**, **Ye C**, **Koda S**, **Fuller PM**, **Krashes MJ**, **Vong L**, **Ray RS**, **Olson DP**, **Lowell BB.** GABAergic RIP-Cre neurons in the arcuate nucleus selectively regulate energy expenditure. *Cell* 151: 645–657, 2012. doi:10.1016/j.cell.2012.09.020.
86. **Morrison SF.** Central control of body temperature. *F1000Res* 5: 880, 2016. doi:10.12688/f1000research.7958.1.
87. **Morrison SF**, **Nakamura K.** Central neural pathways for thermoregulation. *Front Biosci (Landmark Ed)* 16: 74–104, 2011. doi:10.2741/3677.
88. **Matarazzo V**, **Schaller F**, **Nedelec E**, **Benani A**, **Penicaud L**, **Muscatelli F**, **Moyse E**, **Bauer S.** Inactivation of Socs3 in the hypothalamus enhances the hindbrain response to endogenous satiety signals via oxytocin signaling. *J Neurosci* 32: 17097–17107, 2012. doi:10.1523/JNEUROSCI.1669-12.2012.
89. **Ryan PJ**, **Ross SI**, **Campos CA**, **Derkach VA**, **Palmiter RD.** Oxytocin-receptor-expressing neurons in the parabrachial nucleus regulate fluid intake. *Nat Neurosci* 20: 1722–1733, 2017. doi:10.1038/s41593-017-0014-z.
90. **Wu L**, **Meng J**, **Shen Q**, **Zhang Y**, **Pan S**, **Chen Z**, **Zhu LQ**, **Lu Y**, **Huang Y**, **Zhang G.** Caffeine inhibits hypothalamic A1R to excite oxytocin neuron and ameliorate dietary obesity in mice. *Nat Commun* 8: 15904, 2017. doi:10.1038/ncomms15904.
91. **Blevins JE**, **Eakin TJ**, **Murphy JA**, **Schwartz MW**, **Baskin DG.** Oxytocin innervation of caudal brainstem nuclei activated by cholecystokinin. *Brain Res* 993: 30–41, 2003. doi:10.1016/j.brainres.2003.08.036.
92. **Ho JM**, **Anekonda VT**, **Thompson BW**, **Zhu M**, **Curry RW**, **Hwang BH**, **Morton GJ**, **Schwartz MW**, **Baskin DG**, **Appleyard SM**, **Blevins JE.** Hindbrain oxytocin receptors contribute to the effects of circulating oxytocin on food intake in male rats. *Endocrinology* 155: 2845–2857, 2014. doi:10.1210/en.2014-1148.
93. **Carson DS**, **Hunt GE**, **Guastella AJ**, **Barber L**, **Cornish JL**, **Arnold JC**, **Boucher AA**, **McGregor IS.** Systemically administered oxytocin decreases methamphetamine activation of the subthalamic nucleus and accumbens core and stimulates oxytocinergic neurons in the hypothalamus. *Addict Biol* 15: 448–463, 2010. doi:10.1111/j.1369-1600.2010.00247.x.
94. **Angioni L**, **Cocco C**, **Ferri GL**, **Argiolas A**, **Melis MR**, **Sanna F.** Involvement of nigral oxytocin in locomotor activity: a behavioral, immunohistochemical and lesion study in male rats. *Horm Behav* 83: 23–38, 2016. doi:10.1016/j.yhbeh.2016.05.012.
95. **Gao F**, **Zheng KI**, **Wang XB**, **Sun QF**, **Pan KH**, **Wang TY**, **Chen YP**, **Targher G**, **Byrne CD**, **George J**, **Zheng MH.** Obesity is a risk factor for greater COVID-19 severity. *Diabetes Care* 43: e72–e74, 2020. doi:10.2337/dc20-0682.
96. **Guo W**, **Li M**, **Dong Y**, **Zhou H**, **Zhang Z**, **Tian C**, **Qin R**, **Wang H**, **Shen Y**, **Du K**, **Zhao L**, **Fan H**, **Luo S**, **Hu D.** Diabetes is a risk factor for the progression and prognosis of COVID-19. *Diabetes Metab Res Rev* 36: e3319, 2020. doi:10.1002/dmrr.3319.
97. **Jordan RE**, **Adab P**, **Cheng KK.** Covid-19: risk factors for severe disease and death. *BMJ* 368: m1198, 2020. doi:10.1136/bmj.m1198.
98. **Michalakis K**, **Ilias I.** SARS-CoV-2 infection and obesity: common inflammatory and metabolic aspects. *Diabetes Metab Syndr* 14: 469–471, 2020. doi:10.1016/j.dsx.2020.04.033.
99. **Targher G**, **Mantovani A**, **Wang XB**, **Yan HD**, **Sun QF**, **Pan KH**, **Byrne CD**, **Zheng KI**, **Chen YP**, **Eslam M**, **George J**, **Zheng MH.** Patients with diabetes are at higher risk for severe illness from COVID-19. *Diabetes Metab* 46: 335–337, 2020. doi:10.1016/j.diabet.2020.05.001.
100. **Zhou F**, **Yu T**, **Du R**, **Fan G**, **Liu Y**, **Liu Z**, **Xiang J**, **Wang Y**, **Song B**, **Gu X**, **Guan L**, **Wei Y**, **Li H**, **Wu X**, **Xu J**, **Tu S**, **Zhang Y**, **Chen H**, **Cao B.** Clinical course and risk factors for mortality of adult inpatients with COVID-19 in Wuhan, China: a retrospective cohort study. *Lancet* 395: 1054–1062, 2020. doi:10.1016/S0140-6736(20)30566-3.
101. **Hales CM**, **Carroll MD**, **Fryar CD**, **Ogden CL.** Prevalence of obesity and severe obesity among adults: United States, 2017–2018. *NCHS Data Brief* 1–8, 2020.
102. **Das SR**, **Kinsinger LS**, **Yancy WS, Jr**,**Wang A**, **Ciesco E**, **Burdick M**, **Yevich SJ.** Obesity prevalence among veterans at Veterans Affairs medical facilities. *Am J Prev Med* 28: 291–294, 2005. doi:10.1016/j.amepre.2004.12.007.
103. **Ogden CL**, **Carroll MD**, **Kit BK**, **Flegal KM.** Prevalence of obesity in the United States, 2009–2010. *NCHS Data Brief* 1–8, 2012.
104. **Finkelstein EA**, **Trogdon JG**, **Cohen JW**, **Dietz W.** Annual medical spending attributable to obesity: payer-and service-specific estimates. *Health Aff (Millwood)* 28: w822–w831, 2009. doi:10.1377/hlthaff.28.5.w822.
105. **Kusminski CM**, **Bickel PE**, **Scherer PE.** Targeting adipose tissue in the treatment of obesity-associated diabetes. *Nat Rev Drug Discov* 15: 639–660, 2016. doi:10.1038/nrd.2016.75.